Biophysical Journal
Article

Biophysical Society

Interdomain Flexibility within NADPH Oxidase Suggested by SANS Using LMNG Stealth Carrier

Annelise Vermot,[1] Isabelle Petit-Härtlein,[1] Cécile Breyton,[1] Aline Le Roy,[1] Michel Thépaut,[1] Corinne Vivès,[1] Martine Moulin,[2] Michael Härtlein,[2] Sergei Grudinin,[3] Susan M. E. Smith,[4] Christine Ebel,[1] Anne Martel,[2,*] and Franck Fieschi[1,*]

[1]University Grenoble Alpes, CNRS, CEA, Institut de Biologie Structurale, Grenoble, France; [2]Institut Laue-Langevin, Grenoble, France; [3]INRIA, Grenoble, France; and [4]Department of Molecular and Cellular Biology, Kennesaw State University, Kennesaw, Georgia

ABSTRACT Small angle neutron scattering (SANS) provides a method to obtain important low-resolution information for integral membrane proteins (IMPs), challenging targets for structural determination. Specific deuteration furnishes a "stealth" carrier for the solubilized IMP. We used SANS to determine a structural envelope of SpNOX, the *Streptococcus pneumoniae* NADPH oxidase (NOX), a prokaryotic model system for exploring structure and function of eukaryotic NOXes. SpNOX was solubilized in the detergent lauryl maltose neopentyl glycol, which provides optimal SpNOX stability and activity. Using deuterated solvent and protein, the lauryl maltose neopentyl glycol was experimentally undetected in SANS. This affords a cost-effective SANS approach for obtaining novel structural information on IMPs. Combining SANS data with molecular modeling provided a first, to our knowledge, structural characterization of an entire NOX enzyme. It revealed a distinctly less compact structure than that predicted from the docking of homologous crystal structures of the separate transmembrane and dehydrogenase domains, consistent with a flexible linker connecting the two domains.

SIGNIFICANCE We used a detergent adapted to the study of IMPs by SANS to a NOX enzyme, which has limited structural characterization available. We elaborated a strategy involving both SEC-SANS and static SANS to ensure monodispersity of the sample and combined it to contrast variation. We leveraged the property of LMNG detergent that it can be experimentally invisible in SANS, using appropriate buffer, to detect only the deuterated protein contribution. We adapted software to combine SANS data with molecular modeling, providing unique structural information on an entire NOX protein. This work underlines the great potential of the commercial detergent LMNG as a stealth carrier for SANS studies of IMPs. It also reveals the solution structure of this NOX protein and enable to propose function-related flexibility.

INTRODUCTION

More than half of the drugs used in human health target integral membrane proteins (IMPs), including signaling or pathogen attachment receptors, channels, and enzymes. Design of new drugs and therapies greatly benefits from good protein structural information (1), but structure determination of IMPs present a challenge because of their limited recombinant expression, low natural abundance, difficulty of purification, and obstacles to functional study outside their membrane environment. Multidomain IMPs and those that participate in complex assemblies pose even more problems for structural study. Solution NMR is limited to small proteins and is thus rendered unsuitable for many membrane proteins because of the additional size contributed by their solubilizing carrier (bound detergents, amphipathic polymers, nanodisks, etc.). Cryo-electron microscopy is an increasingly powerful solution but again suffers from detergent effects, protein flexibility, and protein size, and the sample is in a frozen state. X-ray crystallography is limited to crystallizable proteins trapped in a unique conformation. Small angle neutron scattering (SANS), though a low-resolution method, fills an important need when investigating conformational changes and/or multicomponent assemblies of IMPs (2).

SANS addresses samples in solution, so IMPs must be solubilized and purified. IMP solubilization uses detergents that shield their hydrophobic transmembrane region from

Submitted January 10, 2020, and accepted for publication June 23, 2020.

*Correspondence: martela@ill.fr or franck.fieschi@ibs.fr

Annelise Vermot and Isabelle Petit-Härtlein contributed equally to this work.

Editor: Michael Sattler.

https://doi.org/10.1016/j.bpj.2020.06.025

aqueous solution. Because detergent can destabilize IMPs, over the last decades, tremendous effort has gone into the development of both new detergents and alternative IMP carrier systems such as nanodisks (3). At first glance, detergent binding presents a problem for SANS because all components—the IMP(s) and the bound detergents (or alternative carrier)—scatter neutrons. Scattering amplitude is related to the neutron scattering length density of each component: protein, detergent, lipid if any, and buffer. The neutron scattering length density (SLD) of a molecule strongly depends on its chemical composition and particularly on its hydrogen content. Through this hydrogen dependence, SANS offers the possibility, by selective deuteration of the solvent and/or components of the membrane protein complex, of masking a specific component. For instance, matching the hydrogen content of the buffer to the detergent can eliminate the scattering signal of the detergent, allowing a focus on the IMP structure. The contrast match point (CMP) of the detergent or carrier is the percent of D_2O in the buffer that provides masking. The heterogeneous structure of lipids and detergents may lead to ordered scattering density fluctuations on a length scale comparable to the macromolecule extension and thus generate residual signals at their CMP. We have shown that this issue can be overcome by using a fluorinated surfactant particularly appropriate for studying membrane multiprotein complexes by SANS (4,5). Recently, another elegant investigation allowed the observation of several conformation states of an ABC transporter using masked "stealth carrier" nanodisks, composed of lipid and membrane scaffold protein (MSP) (6). This approach required solvent with 100% D_2O, 100% deuterated MSP, and selectively deuterated phosphatidyl choline produced using a genetically engineered bacterial strain—a prodigious undertaking inaccessible to most labs (7,8).

Here, we explore the use of lauryl maltose neopentyl glycol (LMNG) as an alternative to these approaches for studying IMPs by SANS. LMNG is an increasingly popular detergent for membrane protein studies (9–11). It is composed of two *N*-dodecyl-β−D-maltoside (DDM) molecules covalently linked at the junction between the hydrophilic and hydrophobic moieties (Scheme S1). LMNG thus contains two acyl chains, like most natural membrane lipids, rendering it much less disruptive to IMPs than classical single-chain detergents, e.g., the reference DDM. We recently demonstrated that LMNG micelles can be experimentally undetectable in SANS in a solvent with 21.4% D_2O (11). This unique feature and the fact that LMNG improves IMP stability make it a good candidate to become a novel versatile stealth carrier for solution studies of IMPs. In these studies, the IMP(s) should be at least partially deuterated, which is reasonably accessible for proteins overexpressed in bacterial and yeast sources.

Our group has long studied NADPH oxidases (NOXes), a family of complex multidomain, and sometimes multicomponent, enzymes (12–14). NOXes are transmembrane flavocytochromes that catalyze the production of reactive oxygen species associated with diverse downstream physiological outcomes ranging from hormone synthesis, balance, cardiovascular tone regulation, and innate immunity. The range of pathologies impacted by NOX make this family a drug target of high value for pharmaceutical companies. We are particularly interested in the neutrophilic NOX complex essential to innate immunity in humans. In the phagocytic cell, NOX2 is activated to generate the "respiratory burst," producing superoxide anion and initiating a cascade of reactions leading to the production of microbicidal hypochlorite. Its activation includes the assembly of several cytosolic components—$p67^{phox}$, $p47^{phox}$, $p40^{phox}$, and Rac—onto the membranous flavocytochome b_{558}. The latter is composed of the catalytic subunit NOX2 and an essential accessory transmembrane subunit $p22^{phox}$ (Fig. 1). Structural information exists for domains or entire proteins of the cytosolic factors (15–22), along with some data regarding association between these cytosolic factors (23). For the transmembrane component of this complex, however, structural data are scarce, and very little is known about how assembly leads to enzyme activity. The SANS signal

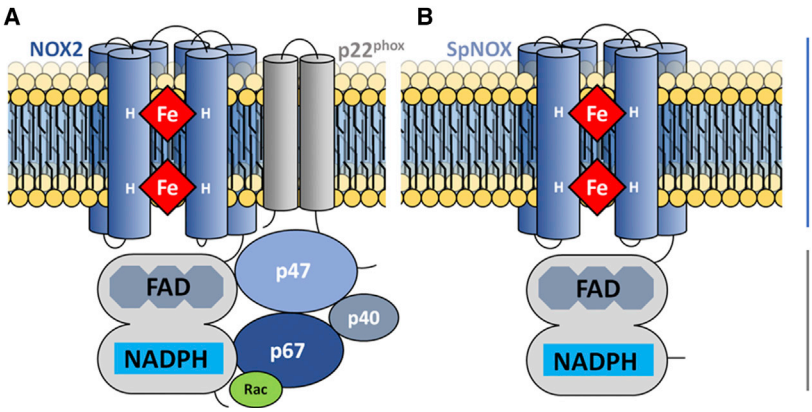

FIGURE 1 Organization of NOX enzymes and related complexes. (*A*) Organization of neutrophilic NOX complex composed of the membrane catalytic subunit NOX2, $p22^{phox}$, and the cytosolic factors $p47^{phox}$, $p67^{phox}$, $p40^{phox}$, and Rac. (*B*) The bacterial NOX from *S. pneumoniae*, SpNOX, a prototype of NOX enzymes, organized into two domains, the heme-containing transmembrane (TM) domain and the cytosolic dehydrogenase (DH) domain containing flavin cofactor and NAD(P)H binding site. To see this figure in color, go online.

matching strategy described above is particularly suited to decipher the structural organization of such a complex. With this objective in mind, a first step before studying such a complex is to find the study conditions compatible with the membrane component.

Recently, we demonstrated the existence of prokaryotic NOXes (24), which we sought as model systems of eukaryotic NOXes with similar structure and function but increased purification yield and stability. Our idea has been well supported; we identified SpNOX, an NOX homolog from *Streptococcus pneumoniae* that expresses well in *Escherichia coli*, yields large amounts of purified protein, and remains active in detergent solution (24). The main difference between SpNOX and its eukaryotic counterpart resides in its independence from additional factors for activity. Otherwise, as with the eukaryotic NOXes, SpNOX is composed of two domains: a transmembrane (TM) cytochrome that binds two hemes, and a cytosolic dehydrogenase (DH) domain that holds an FAD molecule and binds the NAD(P)H electron donor (Fig. 1). Despite significant effort, we have not yet succeeded in obtaining crystals of full-length SpNOX diffracting at high resolution. Another group recently provided the most complete crystal structures for the NOX family when they separately crystallized the TM and DH domains of CsNOX, an NOX5 homolog from cyanobacteria (25). Docking of the two separate domains provides a model of the entire protein, but even so, to date no crystal structure of an entire NOX has been obtained. SANS characterization of SpNOX can provide new information regarding the structural specificities of the full-length enzyme.

Here, we thus used the SpNOX protein as a prototype NOX family member for SANS structural investigation. We recently showed that SpNOX is obtained with an improved homogeneity in LMNG compared to DDM and that it shows a significantly increased specific activity and melting temperature in LMNG compared to DDM (11). Using NanoDSF, we confirmed LMNG as the detergent providing the highest stability for SpNOX among the commercially available members of the neopentyl glycol detergents. We screened conditions to establish the best combination for both structure stability and activity of SpNOX and elaborated an SANS strategy involving both size exclusion chromatography (SEC)-SANS and static SANS to ensure homogeneity and monodispersity of the sample. We confirmed scattering of LMNG micelles, and buffer can be rendered indistinguishable by use of an appropriately deuterated buffer, thus entirely matching out the LMNG contribution to the SANS signal. This is despite the heterogeneity in chemical composition of the hydrophobic and hydrophilic moieties of LMNG (their SLDs are reported in Table S1). It allows us uniquely to detect the deuterated protein contribution. We adapted Pepsi-SAXS software to combine SANS data with normal mode analysis and provided a first, to our knowledge, structural characterization of an entire NOX enzyme. Unexpectedly, we saw that the TM and DH domains are not in the tight interaction previously proposed and that the close contact between the two domains required for the electron transfer implies that the DH domain can move relative to the TM domain. This leads us to propose a certain flexibility of the interdomain linker. This work underlines the great potential in the use of the LMNG micelle as a general stealth carrier for future SANS studies of IMPs. It also reveals that the conformation of the entire NOX enzyme shows differences from the conformation expected from the structures of its two isolated domains, demonstrating the complementarity between high- and low-resolution techniques.

MATERIALS AND METHODS

Cloning and expression of hydrogenated and deuterated His-SpNOX

The synthetic SpNOX gene optimized for expression in *E. coli*, including polyhistidine tag and thrombin cleavage site, was amplified via PCR and subcloned into pET-30b (Novagen, Madison, WI) between the NdeI/BamHI sites. Unlabeled His-SpNOX was induced in *E. coli* C41(DE3), grown in lysogeny broth medium supplemented with 50 mg L^{-1} kanamycin, by addition of 0.2 mM isopropyl β-d-1-thiogalactopyranoside (at A_{600} of 1.2), followed by culture for 3.5 h at 37°C. Cells were harvested by centrifugation. Using the same expression system, 74% deuterated His-SpNOX was produced in the Institut Laue-Langevin Deuteration Laboratory (D-Lab), Grenoble, France, following established protocols for high cell-density cultures in deuterated minimal medium (26,27). After adaptation of cells to deuterated minimal medium (28), a 100 mL flask culture was grown in Enfors medium containing 85% D_2O, 5 g L^{-1} unlabeled glycerol, and 35 mg L^{-1} kanamycin to inoculate a fermenter culture in a 3 L fermenter (Labfors 2; Infors, France). During the batch and fed-batch phases, the pH/D was adjusted to 6.9 by addition of NaOD (Eurisotop, Saint-Aubin, France) and the temperature was adjusted to 30°C. When the A_{600} reached a value of ~12, His-SpNOX expression was induced by 0.5 mM isopropyl β-d-1-thiogalactopyranoside and pursued for 20 h. Cells were then harvested and stored at −80°C. From two fermenter runs, 108 g (wet weight) of deuterated cell paste were obtained.

His-SpNOX purification

Membrane preparations were performed as described previously (24). Membrane pellets (typically 12 × 1 mL aliquots each containing 20 mg protein) were solubilized to 0.6 mg mL^{-1} in 50 mM Tris-HCl (pH 7), 300 mM NaCl, 5 mM (0.5%) LMNG (NG310-MNG; Anatrace, Maumee, OH), and 10 μM FAD (unless otherwise noted), incubated overnight with shaking at 4°C. Insoluble material was removed by ultracentrifugation at 105,000 × *g* for 45 min at 4°C. The two-step purification, done at 4°C, was automated on an Akta Xpress (GE Healthcare, Chicago, IL); the solubilized supernatant was loaded on a 1 mL equilibrated HisTrap HP Prepacked Column (GE Healthcare); the column was washed with 50 mM Tris-HCl (pH 7), 300 mM NaCl, 0.1 mM LMNG, 10 μM FAD, 90 mM imidazole. The protein was eluted with 0.025 mM LMNG and 300 mM imidazole in the same buffer. The 4 mL elution peak was then automatically loaded on a HiLoad 16/600 Superdex 200 column (GE Healthcare) previously equilibrated with 50 mM Tris (pH 7.0), 300 mM NaCl, and 0.025 mM LMNG. The SEC profile displays a main peak corresponding to His-SpNOX monomer. The selected fractions were concentrated by ultrafiltration (Amicon Ultra-4 (Sigma-Aldrich, St. Louis, MO), cutoff 50 kDa). When decyl maltose neopentyl glycol (DMNG) or DDM was used as a detergent, the same purification protocol was followed but with adjustment of detergent concentrations in the buffers. Those were

previously described for DDM (11). In the case of DMNG, detergent concentrations were 5.3 mM in the solubilization buffer and 0.21 mM for the elution buffers of the Ni-HisTrap and the SEC columns.

His-tag cleavage

We used commercial thrombin immobilized on agarose (Thrombin CleanCleave Kit; Sigma-Aldrich). The manufacturer's protocol was adapted to increase the cleavage yield: the resin was washed thrice by centrifugation in the cleavage buffer, 200 μL of packed resin was resuspended with 700 μL of 10× cleavage buffer, and 6 mL SpNOX at 0.1 mg mL^{-1} were added before incubation overnight at 4°C on a rotating wheel. The cleaved protein, named Tagfree-SpNOX, was recovered by gravity, and its solvent was exchanged on a desalting column (PD10 colum ref 17-0851-01; GE Healthcare) before concentration.

Thermostability studies using NanoDSF instrumentation

Thermal stability assays were performed using a Prometheus NT.48 instrument (NanoTemper, Germany). 50 μL of sample per condition were prepared to perform experiments in triplicates. Standard-treated glass capillaries filled by capillarity with 10 μL of sample were loaded into three sets of 16-capillary sample holders yielding up to 48 conditions inserted into the instrument. The excitation at 280 nm was optimized to yield emission intensities of intrinsic fluorescence of tryptophan at 330 and 350 nm, in the absence of heat gradient, in the range of 5000 and 16,000 relative arbitrary units. The temperature gradient was set to an increase of 1°C min^{-1} in a range from 15 to 95°C. Protein unfolding was measured by detecting the temperature-dependent change in the ratio of fluorescence emission at 350 vs. 330 nm. Protein aggregation was detected by measuring the intensity of back-scattered light. The fluorescence ratio versus time was fitted with eighth-order polynomial function and the first derivative of this function. The melting temperature was then determined by detecting the maximum of the first derivative of the fluorescence ratio. Repeatability of experimental results revealed an accuracy of the melting temperature extracted by this method of $\pm$1.5°C (Supporting Material). Test of pH impact on the protein stability used concentrated SpNOX solution (8 mg mL^{-1}) diluted 10 times in the following 0.1 M buffers: citric acid for pH 4, 5, 5.5, and 6; sodium acetate for pH 4.5; bis tris-propane for pH 6.5 and 8, Pipes for pH 7; Tris for pH 7 and 7.5; bicine for pH 9; and CAPS (*N*-cyclohexyl-3-aminopropanesulfonic acid) for pH 9.5. In all cases, LMNG concentration was 0.025 mM.

Enzymatic activity assay

Cytochrome c was used as a reporter of superoxide production by SpNOX. SpNOX activity was monitored by following superoxide's reduction of cytochrome c reduction at 550 nm, as previously described (24). Briefly, 10 μM FAD and 100 μM cytochrome c were added to 1 μg of protein in a 1 mL reaction volume in the buffer corresponding to the conditions tested (see previous section on Thermostability Studies Using NanoDSF Instrumentation). The extent of cytochrome c reduction was calculated based on the absorbance difference at 550 nm with an absorption coefficient of 21,000 M^{-1} cm^{-1}. The reaction was initiated by the addition of 200 μM NADPH, and the temperature was kept at 25°C. Results are expressed as moles of reduced cytochrome c per mole of SpNOX per second.

Data analysis of thermostability and activity assays

The results from thermostability and activity assays were analyzed simultaneously using the JMP statistical software (version 13.0; SAS Institute, Cary, NC) to plot two-dimensional (2D) contour plots of T_m and activity as a function of pH and salt concentrations. The median of triplicates was used to produce the charts, and linear interpolations were done in between measurement points to fill the charts. A 2D linear interpolation was performed on thermostability and activity results as a function of pH and salt concentration, using Python to produce a three-dimensional (3D) chart (see Fig. S5).

Structure-based sequence alignment

A large set of 549 NOX homolog sequences distributed about evenly between prokaryotes and eukaryotes were aligned using MAFFT (29). The sequences were split into TM and DH domains, identified by homology. Each domain was realigned separately with Promals3D (30). The TM alignment was constrained to the crystal structure of CsNOX TM domain (PDB: 5O0T), whereas the DH alignment was constrained to the crystal structure of CsNOX DH domain (PDB: 5O0X) and DH domain homologs PDB: 1GJR, 1FNB, 1GVH, 2EIX, 3A1F; all other parameters were at default values. The resulting multiple alignments were inspected in Jalview (31); those with missing secondary structural elements or with unusually large insertions were discarded and remaining sequences were pruned to 91% (TM domain) or 95% (DH domain) identity. The final sequence sets (TM domain: 172 sequences and DH domain: 207 sequences) were realigned in Promals3D with default parameters and the same structural constraints as specified above.

Homology model generation

The sequences of the SpNOX TM and DH domains were independently submitted for structural modeling to the I-TASSER server (32). For the TM domain, we constrained I-TASSER with the TM domain of CsNOX. I-TASSER identified PDB: 4EH1 (FAD/NAD binding domain of nitric oxide dioxygenase) as the closest homolog to the SpNOX DH domain. Resulting models were visualized and structurally superimposed onto the corresponding CsNOX crystal structures using Chimera (33). The D-loop of the SpNOX TM model was reconstructed using Superlooper (34) with A^{110} and W^{121} as N-terminal and C-terminal anchors, respectively. The highest scoring loop with similar orientation to that of CsNOX was accepted. The homology model including the remodeled D-loop was compared to the structure of CsNOX TM domain in Chimera via the Matchmaker tool with default values. The homology models of the TM and DH domains of SpNOX were docked together by structurally aligning each domain to the docked structures of the CsNOX TM and DH crystals (25) using the Chimera Matchmaker feature; the docked CsNOX structure was generously provided by Dr. Magnani. For His-SpNOX modeling, the initial His-tag structure was generated using the online tool QUARK (https://zhanglab.ccmb.med.umich.edu/QUARK/) (35,36).

SANS samples and measurements

SpNOX SANS signal was measured using two sample environments on ILL SANS-D22. For static measurement, using the classical 22-position sample changer, His-SpNOX was prepared according to the following protocol: after the preparative SEC, fractions corresponding to a monomeric form were pooled. Fractions contaminated with a dimeric form were combined, concentrated, and reinjected on Superdex 200 10/300, to recover a second pool of monomer fractions. The two monomer pools were mixed, concentrated, and injected on Superdex 200 equilibrated with a buffer containing 21.4% D_2O (100 mL was prepared). All monomer fractions but one was pooled and concentrated by a factor of ~7 to A_{280} = 3.36 before SANS measurement. One fraction (A_{280} = 1.23) was measured in SANS without further treatment for comparison. The Tagfree-SpNOX was prepared in the same way, except that the thrombin cleavage was performed before the last

SEC in 21.4% D_2O, leading to a sample with $A_{280} = 2.98$. The SANS signal of these samples was measured in Hellma suprasil quartz cells (Hellma, Müllheim, Germany) 100QS with 1 mm optical pathlength. The sample temperature was kept at 7°C during the exposure times. Scattering data were recorded at two instrumental detector/collimator configurations, 2 m/2.8 m and 5.6 m/5.6 m, using a neutron wavelength of $\lambda = 6$ Å $\pm$ 10%. At each instrumental configuration, the neutron flux reaching the sample was precisely measured, as well as the direct beam transmission, the scattering of a boron-enriched material, and the scattering and transmission of an empty cell of all buffers and of all samples. The exposure times varied between 20 and 120 min. Data are scaled to absolute intensity using direct beam flux.

For measurement by SEC-SANS (37), 11 mL of His-SpNOX from the preparative SEC (see above) were concentrated to obtain 270 μL of protein at 7.5 mg mL^{-1}, and a volume of 250 μL was injected at 12°C on a Superdex 200 Increase column (GE Healthcare) of the SEC-SANS setup. The equilibration buffer was 50 mM Tris-HCl (pH 7), 300 mM NaCl, 10 μM FAD, 0.025 mM LMNG, and 21.4% D_2O (200 mL was prepared). An intermediate configuration is used to cover the Guinier range of the curve: 4 m collimation and 4 m sample-detector distance, still with a wavelength of $\lambda = 6$ Å $\pm$ 10%. Individual patterns of an exposure time of 30 s were continuously recorded along the elution and averaged later to generate sample and buffer patterns. Calibration, data corrections, and reduction are the same as for SANS in cuvette. Ultraviolet (UV) was acquired at 280, 416 (maxima of absorption of SpNOX), 380, and 450 nm. Fractions of 10 drops ($\sim$0.89 mL) were collected.

SANS data reduction

Curves of scattering intensity I(q) in absolute scale (cm^{-1}) vs. q (where $q = 4\pi\sin\theta/\lambda$, 2θ is the scattering angle, and λ is the neutron wavelength) were obtained as follows. The neutron flux at sample position was used to calibrate scattering intensity to absolute scale. The empty beam transmission was used to set the center of the patterns and to calculate the transmission of the empty cell, the buffers, and the samples. The scattering of the piece of boron-enriched material, absorbing the totality of the beam flux, was subtracted from all other patterns because it results from ambient and electronic noise. The raw data were reduced (detector efficiency, electronic and empty cell background subtraction, angular averaging, transmission, and thickness correction) using GRASP software package (https://www.ill.eu/users/support-labs-infrastructure/software-scientific-tools/grasp/). The scattering curves measured at the two different configurations and covering different but overlapping q ranges were merged after respective buffer subtraction using SANS reduction macros written by S. Kline for Igor software (38). To continue the analysis, using the ATSAS suite of software, the resolution column and data at $q > 0.25$ $Å^{-1}$ were removed, and the q-values were expressed in nm^{-1}. The radii of gyration (Rg) and the intensities scattered in the forward direction (I(0)) of all samples were extracted by the Guinier approximation, with $Rg \times q \leq 1.3$, using the program Primus (39).

SANS data analysis

Ab initio shape reconstruction was applied to two sets of data corresponding to the concentrated His-SpNOX sample ($A_{280} = 3.36$) and Tagfree-SpNOX ($A_{280} = 2.98$), selected for their high signal/noise ratio, after careful quality control and comparison with SANS signal from less concentrated samples. The ATSAS suite was used to generate an ab initio shape from each data set according to this work flow (40) (kindly provided by Dr. Cy Jeffries): for each data set, GNOM (41) was used to calculate the pair distance distribution function of the particle, $p_{(r)}$, imposing a maximum distance $D_{max} = 10$ nm and the restraints $p_{(r = 0)} = 0$ and $p_{(r = Dmax)} = 0$. DAMMIN online (www.embl-hamburg.de/biosaxs/atsas-online/) generated 20 independent shapes which were compared using CorMap. Being all similar enough (p-value = 1), they were selected using DAMSEL and superimposed, averaged, and filtered using successively DAMSUP, DAMAVER, and DAMFILT (42). The NSD (normalized spatial discrepancy) from the damsel.log file being smaller than 1, DAMSTART generated the input file for refinement using DAMMIN in expert mode, imposing 25 harmonics and 80 knots. The envelops presented in Fig. 7 are the results of this refinement procedure.

For the model-based analysis, the program Pepsi-SANS was used online, in its "flexible fit" option, to tune our homology model to fit the SANS data, keeping fixed the TM domain fixed from the N-terminus to the Y191. This software can rapidly generate a multitude of models along the slowest normal modes computed for the starting structure (32), calculate their scattering curves, and compare them with experimental data (after smearing them by the instrumental resolution). Its approach follows the observation that most protein functional motions can be well described with just a few collective coordinates computed using the normal mode analysis (43). Adapted from Pepsi-SAXS (31) to SANS data (absolute intensity and experimental smearing), Pepsi-SANS software can be downloaded at https://team.inria.fr/nano-d/software/pepsi-sans/ or used online at https://pepsi.app.ill.fr/ to calculate scattering profiles from a crystallographic structure or model in pdb format.

Software, parameters, and main results of this analysis are provided in Table S3, adapted from Trewhella et al. (44), and the structures have been deposited to the Small Angle Scattering Biological Data Bank (SASDBD) under SASDJ63 (Tagfree-SpNOX).

SEC-LS

SEC-LS experiments were conducted at 4°C on an HPLC consisting of a degasser DGU-20AD, a LC-20AD pump, an autosampler SIL20-AC_{HT}, a communication interface CBM-20A, and a UV-Vis detector SPD-M20A (Shimadzu, Kyoto, Japan), a column oven XL-Therm (WynSep, Sainte Foy d'Aigrefeuille, France), a static light scattering miniDawn Treos, and a refractive index Optilab rEX detector (Wyatt, Santa Barbara, CA). The analysis was made with the software ASTRA, v5.4.3.20 (Wyatt). Samples of 100 μL of F12, F13, and F14 from the SEC-SANS experiment were injected at 0.5 mL min^{-1} on a Superdex 200 10/300 GL (GE Heathcare) equilibrated with 50 mM Tris-HCl (pH 8), 300 mM NaCl, 10 μM FAD, 0.025 mM LMNG. Bovine serum albumin at 2 mg mL^{-1} in phosphate-buffered saline buffer was injected as a control.

Numerical values used for SEC-LS and SANS analysis

The calculated molar masses of His-SpNOX and Tagfree-SpNOX are 48.081 and 46.527 kDa, respectively. Estimating the absorbance coefficient of a detergent- solubilized membrane protein that contains both heme and FAD can be very complex. We used quantitative acid hydrolysis: weighed samples of two independently purified preparations of His-SpNOX and Tagfree-SpNOX of known absorbance at 280 nm (each at three dilutions) were subjected to acid hydrolysis for 24 h at 100°C, and quantitative amino acid analysis was performed in a Biochrom 30 (Biochrom, Cambridge, UK). The derived extinction coefficients at 280 nm were 97,527 and 116,604 M^{-1} cm^{-1}. The extinction coefficient varies from sample to sample because of uncontrolled differences in sample preparation. We chose the mean value of 107,066 M^{-1} cm^{-1} $\pm$ 10% (i.e., 2.227 and 2.301 (mg mL^{-1})$^{-1}$ cm^{-1} for His-SpNOX and Tagfree-SpNOX, respectively). This value, within 10% error, should be considered with respect to the theoretical value due to the contribution of the protein alone (68,760 M^{-1} cm^{-1} from Expasy Protparam online). The true value lies somewhere between these two values and depends greatly on the heme and FAD contribution in this protein context, as well as the ratio of apoprotein to holoprotein in the sample. To provide an order of magnitude of the errors associated with extinction coefficient uncertainties, molar masses from the forward

intensity are reported in Table S3 using our experimental extinction coefficient, along with that of the protein contribution alone.

His-SpNOX concentration in the SEC-SANS profiles was estimated as c (mg mL^{-1}) = 1.315 A_{450}, derived from the extinction coefficient at 280 nm and the absorbance spectrum of an eluted fraction.

The refractive index increment $\partial n/\partial c = 0.1938$ mL g^{-1} and partial specific volume $\overline{V} = 0.75$ mL g^{-1} were calculated from amino acid sequence in the program Sedfit (freely available at https://sedfitsedphat.nibib.nih.gov/default.aspx). For LMNG, $\partial n/\partial c = 0.146$ mL g^{-1} (11).

The deuteration level is 70% of the nonlabile hydrogens as measured by MALDI-TOF. For SLD and I(0) calculation, the BSLDC calculator online (http://psldc.isis.rl.ac.uk/Psldc/) was used, assuming an exchange rate of 80% for the labile hydrogens. The protein SLD is 5.178 10^{10} cm^{-2}, and the SLD of the buffer is 0.929 10^{10} cm^{-2}.

RESULTS AND DISCUSSION

Optimization of SpNOX sample

We determined the thermostability and aggregation propensity of purified His-SpNOX in a range of conditions to find optimum buffer conditions for SANS using nanoDSF technology. We simultaneously followed the ratio of the fluorescence emitted at 350 and 330 nm (F350/F330) and light back scattering; F350/F330 reports the protein folding state, from which melting temperature (T_m) is extracted, whereas light back scattering reports protein aggregation. From a preliminary set of measurements at different protein concentrations (range 0.8–8.2 mg mL^{-1}), the SpNOX concentration was found to greatly impact the unfolding curve appearance and thus the extracted melting temperature (T_m) because of concomitant aggregation (Figs. S1 and S2). As a compromise, the working concentration for further experiments was set close to 1 mg mL^{-1}.

Detergent screening for optimal stability and minimal aggregated state

The choice of detergent is crucial to maintain the stable structure of membrane proteins (45). In addition, for studying IMPs in SANS, the detergent should allow good cancellation of its scattering contribution. In the fluorinated detergent F6-DigluM, previously characterized in our group to be entirely masked at its match point (5), SpNOX was inactivated and aggregated (data not shown). LMNG, which also presents a matching point allowing good cancellation of its scattering contribution in SANS (11), was identified as a good detergent for SpNOX (11,24). This makes the maltose neopentyl glycol detergent class of particular interest. LMNG possesses two linked lauryl chains. However, DMNG, with reduced aliphatic chains, which leads to a smaller detergent belt, may offer a promising alternative. We thus assessed the stability of His-SpNOX in LMNG, DMNG, and also DDM as a reference. As shown in Fig. 2, His-SpNOX purified in LMNG has a Tm 9°C higher than DMNG and 20°C higher than DDM. Similarly, an improved aggregation temperature (T_{agg}) was noticed for LMNG, 21°C higher than DMNG and 25°C higher than DDM. According to these results, LMNG is confirmed as the most appropriated detergent to promote the overall stability of SpNOX for biophysical studies.

Salt and pH screen to optimize SpNOX thermostability

Changes in pH and salt concentrations can modulate the charges within proteins (46), thus influencing protein stability. His-SpNOX thermostability was assessed through wide ranges of pHs and salt concentrations. The thermal unfolding curves monitored show an increase of T_m with increasing NaCl concentrations or decreasing pHs. Fig. 3 shows a 2D contour plot combining the influence of both pH and salt concentration on SpNOX stability and demonstrates the existence of a thermostable plateau for pH $<$ 7 and [NaCl] $>$ 200 mM with T_m higher than 60°C. Experiments using back scattering to monitor aggregation in the same conditions gave similar results (Fig. S3).

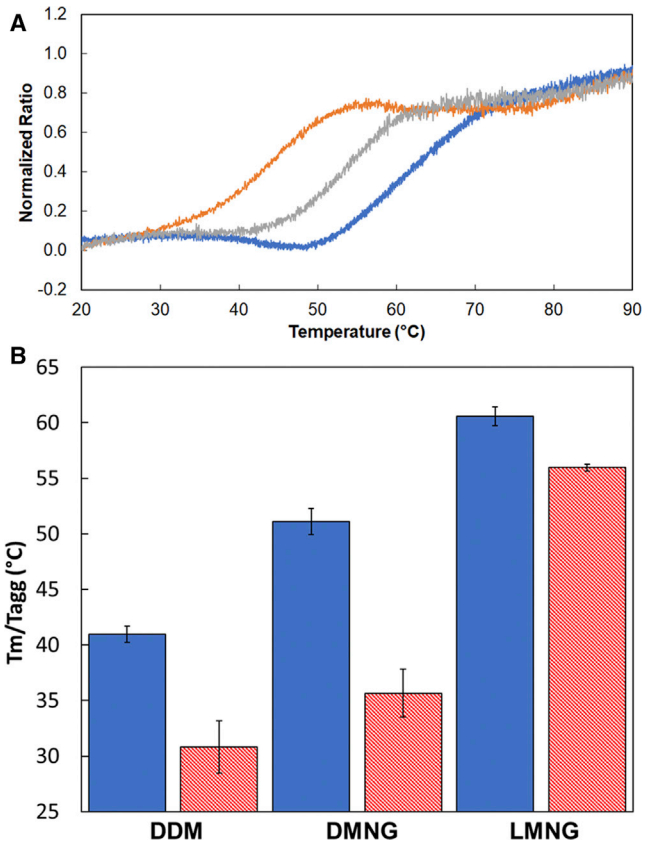

FIGURE 2 Optimization of SpNOX thermostability in detergent. (*A*) Normalized thermal unfolding curves of His-SpNOX (0.8 mg mL^{-1}) in the presence of 300 mM NaCl for several detergents: DDM (*orange*), DMNG (*gray*), and LMNG (*blue*). (*B*) A summary of T_m (°C) (*blue*) and T_{agg} (°C) (*red*) measured for DDM, DMNG, and LMNG. Standard errors are represented as the result of experiments done in triplicate. To see this figure in color, go online.

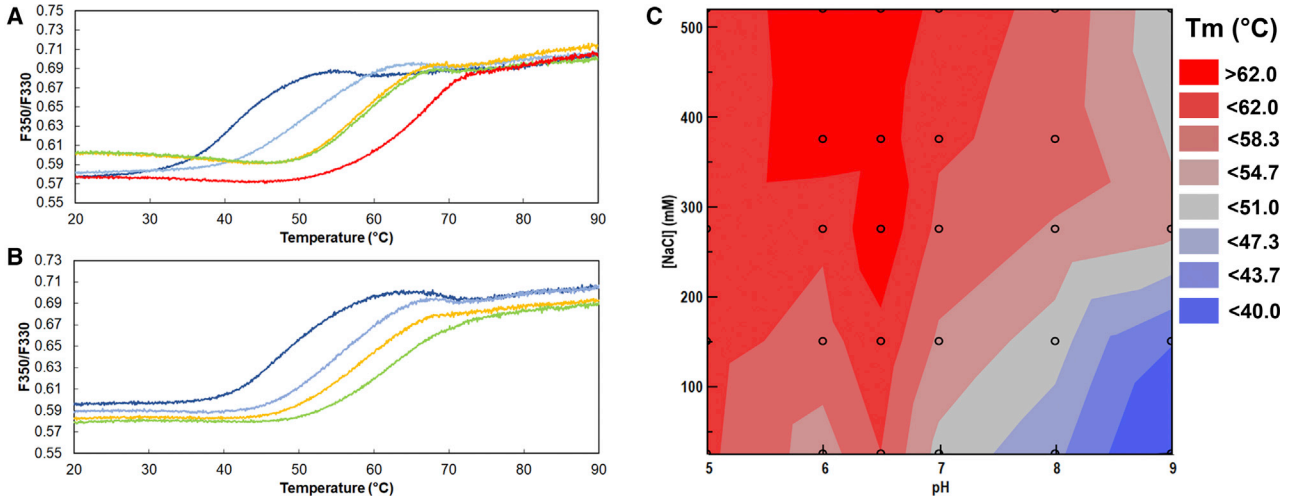

FIGURE 3 Optimization of pH and salt concentration to promote SpNOX thermostability. (*A*) Thermal unfolding curves of SpNOX (0.8 mg mL^{-1}) in buffers containing 300 mM NaCl with various pHs: (*dark blue*) pH 9, (*light blue*) pH 8, (*orange*) pH 7, (*green*) pH 6, and (*red*) pH 5. (*B*) Thermal unfolding curves of His-SpNOX (0.8 mg mL^{-1}) in elution buffer at pH 7 with NaCl concentrations of (*dark blue*) 25 mM, (*light blue*) 150 mM, (*orange*) 275 mM, and (*green*) 520 mM. (*C*) A 2D contour representation of T_m dependence with pH and NaCl concentrations. Open symbols represent experimental data. To see this figure in color, go online.

Maximizing SpNOX activity

We monitored the activity of SpNOX in a range of salt and pH conditions. Fig. 4 shows the activity of His-SpNOX in the same conditions of salt and pH as in Fig. 3. The 2D contour plot of specific activity as a function of salt concentration and pH emphasizes the existence of a clear optimum at pH 7 and 250 mM NaCl, with progressive loss of activity with increasing distance from the optimum (Fig. 4 *C*). FAD from 0.01 to 100 μM had essentially no effect on the thermostability of SpNOX (see Fig. S4). However, because supplementation with FAD was previously shown to be necessary for full activity of SpNOX (24) and, because of its potential lability, to further strengthen the equilibrium in favor of FAD containing SpNOX, this cofactor was included; combined thermostability and activity analysis (integrated in Fig. S5) allowed us to define an optimum buffer composition for SpNOX used throughout the

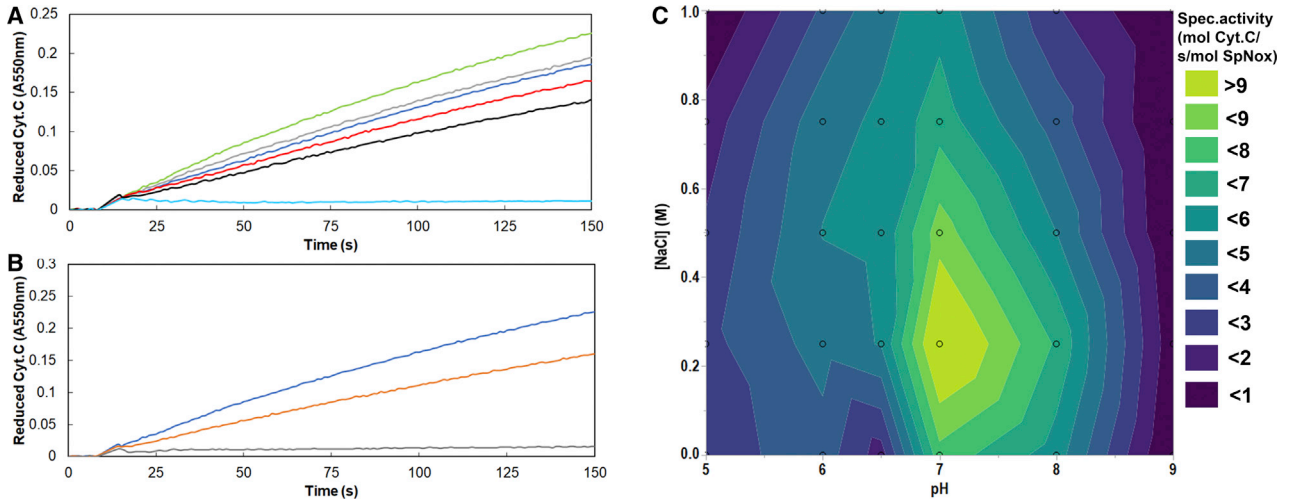

FIGURE 4 Optimization of salt concentrations and pH to promote SpNOX cytochrome c reductase activity. (*A*) Monitoring of cytochrome c reduction in presence of SpNOX (1 μg), NADPH (200 μM), and FAD (10 μM) in the elution buffer at pH 7 in the presence of various NaCl concentrations: (*blue*) 25 mM, (*green*) 250 mM, (*gray*) 500 mM, (*red*) 750 mM, and (*black*) 1 M. The curve in cyan represents a control containing all reactants except SpNOX. (*B*) Monitoring of cytochrome c reductase activity with SpNOX (1 μg), NADPH (200 μM), FAD (10 μM), and NaCl (300 mM) at varying pH: (*gray*) pH 9, (*orange*) pH 8, and (*blue*) pH 7. (*C*) 2D contour representation of cytochrome c reductase specific activity dependence with pH and NaCl concentration. Specific activities are represented using a color scale corresponding to values expressed as mole of reduced cytochrome c per mole of protein per second. Open symbols represent experimental data. To see this figure in color, go online.

study: 50 mM Tris-HCl (pH 7), 300 mM NaCl, 10 μM FAD, 0.025 mM LMNG.

SANS and SEC-SANS for deciphering the low-resolution SpNOX structure

We then investigated the general structure of SpNOX in solution using SANS. To increase the contrast between hydrogenated proteins (calculated CMP ~44% D_2O) and LMNG (experimental CMP ~21.4% D_2O), we produced SpNOX in a deuterated form (calculated CMP ~100% D_2O). All the SANS experiments described below were performed with the deuterated protein. His-SpNOX was overexpressed in 85% D_2O; after solubilization and purification, the deuterated SpNOX had the same homogeneity and properties (absorption spectrum, specific activity) as the hydrogenated protein. MALDI-TOF was used to estimate the deuteration level of nonlabile hydrogens, which was found to be 70% (Table S2). Sample monodispersity is essential in SANS because the scattering curve results from the scattering of all particles in solution. SEC-SANS was recently described (37) to improve SANS data collection for complex sample, providing data of sufficient signal/noise ratio while at the same time circumventing aggregation.

SEC-SANS experiments

The use of SEC-SANS was motivated by SpNOX's moderate stability and the evidence of minor amounts of aggregates after purification (11). Before injecting SpNOX, we first checked that the scattering of LMNG is indistinguishable from that of the buffer at its CMP, despite the chemical heterogeneity of its hydrophobic and hydrophilic moieties (Scheme S1; Table S1). Fig. 5 *B* reports the raw scattering measured at a low angle after injection of LMNG at 25 mM in the buffer containing 21.4% D_2O. We know that LMNG injected at 20 mM elutes as a very large peak between 10 and 15 mL, with a maximum at 12 mL (11). LMNG is thus clearly undetected. SpNOX in the last SEC purification step appears essentially homogeneous, but a left shoulder indicates aggregated species (Fig. 5 *A*). To avoid contamination by aggregates, SpNOX fractions of the second part of the main peak were pooled and concentrated to 7.5 mg mL^{-1} before injection on the SEC column coupled to SANS. The chromatograms at 450 nm and for the scattering signal at low angle were superposed in Fig. 5 *C*. The flow rate was decreased when the protein came off the column to increase the SANS signal/noise ratio for the homogeneous protein. The normalized scattering profiles from UV and SANS are nearly superimposed. A shoulder was still detected before the main SpNOX peak (Fig. 5 *C*); its scattering/UV ratio is twofold that of the main peak, as observed in Fig. 5 *C* comparing the scattering and UV signals at ~26 and ~36 mL, indicating that the shoulder corresponds to a dimer of the species present in

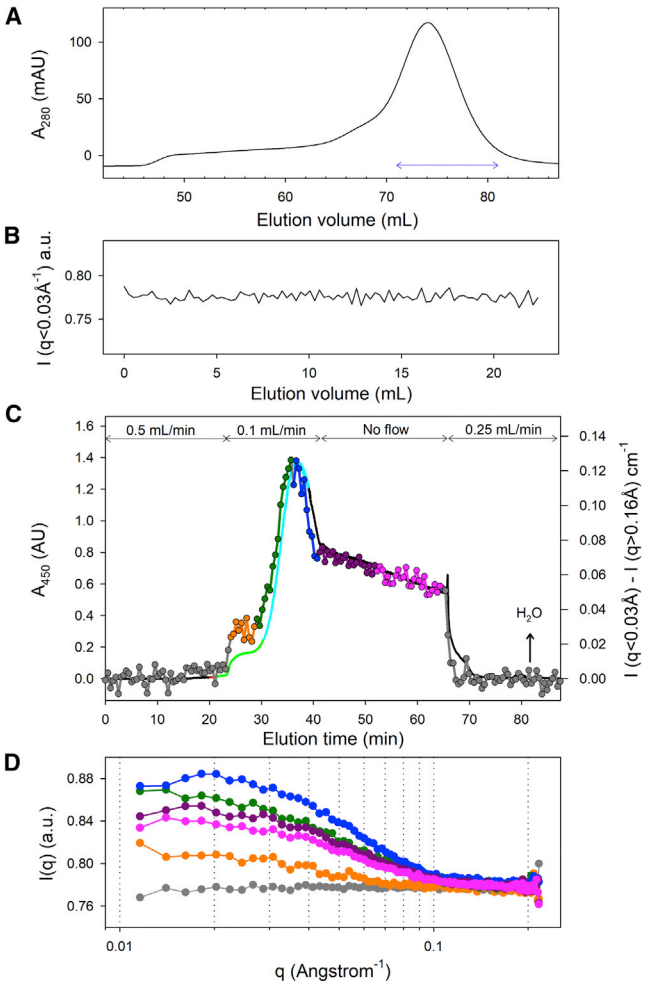

FIGURE 5 SEC-SANS experiment. (*A*) Preparative SEC profile of SpNOX, eluted on a HiLoad 16/600 Superdex 200 column, in 50 mM Tris-HCl (pH 7), 300 mM NaCl, 10 μM FAD, and 0.025 mM LMNG. Fractions indicated by the blue arrow were pooled and concentrated for SEC-SANS. (*B*) SEC-SANS of LMNG: sum of the neutron counts measured at low angle for 250 μL of 25 mM LMNG injected on a Superdex 200 10/300 coupled to SANS as a function of elution volume. Elution buffer and sample contained 21.4% D_2O. (*C*) SEC-SANS profiles for 250 μL of 7 mg mL^{-1} SpNOX injected on the same column with the same buffer: absorbance at 450 nm (*black line*) and scattering intensity difference between the low and large angles (*gray line*) as a function of elution time. Water elution volume was determined by its incoherent scattering (not visible in this graph), measured as an equal increase in the low and large angle counts. The flow rates are indicated on the top part of the panel. The chromatograms show an anomalous decreasing plateau at the right of the main peak; it is clear that an air bubble was trapped, and the flow rate decreased. The approximate elution volumes for fractions 12 (*red*, at ~20 min elution, hardly seen on the plot because of the large flow rate), 13 (*green*), and 14 (*cyan*) are indicated on the A_{450} profile. Profiles recorded at 280, 380, and 416 nm showed absorbance >2. The data selected for averaging and named box 1 (*orange*), 2 (*dark green*), 3 (*dark blue*), 4 (*dark pink*), and 5 (*pink*) are indicated by colored lines and circles on the SANS profile. (*D*) Averaged scattering curves of SpNOX from SEC-SANS experiment. The colors are those of the boxes defined in (*C*), except the elution buffer (*gray*). To see this figure in color, go online.

the main peak. The approximate elution times of the collected fractions 12, 13, and 14 are displayed in Fig. 5 *C*. They were analyzed 4 and 5 days after the SANS experiments by absorbance, SEC-LS, specific activity, MALDI-TOF, SDS-PAGE, and thin-layer chromatography. Results are shown in Table S2. SEC-LS indicates fractions F12 and F13 contain a significant proportion of dimer, whereas fraction F14 is essentially homogeneous with 94% monomer. Its specific activity is similar to that of hydrogenated SpNOX in the hydrogenated version of the buffer (8 vs. 9.2 mol cytochrome c reduced s^{-1} mol^{-1} SpNOX; see above and (11)) (Fig. S6; Table S2). SpNOX monomer binds 1.6 g g^{-1} LMNG, in agreement with previously published estimates (11). From the A_{416}/A_{280} ratio and specific activity, the protein has the appropriate heme content and is fully active. The scattering profiles were averaged first in five "boxes," indicated by colors on the SANS profile on Fig. 5 *C*. The resulting average raw data are shown in Fig. 5 *D*. The radii of gyration, Rg, and mean molar masses derived from Guinier plots are larger for boxes 1 and 2 (Rg of 34 and 31 Å and molar masses of 110 and 70 kDa, respectively) than for boxes 3–5, in which the values are constant. We thus averaged all the data corresponding to boxes 3–5, representing 28 min of measurement, with a mean concentration of 1.05 mg mL^{-1}. Average values yielded Rg = 28.1 ± 0.8 Å and a molar mass of 49 ± 1 kDa, in agreement with the monomer value of 48 kDa.

Static SANS experiments

Because SEC-SANS experiments can measure SpNOX at only moderate concentration and because we demonstrated that the monomer can be obtained from SEC and preserved without dimer contaminant for hours, we decided to measure the scattering of the monomer of SpNOX in the usual static SANS configuration. His-SpNOX monomer was obtained from successive SEC, the last elution using a 21.4% D_2O buffer, and followed by concentration via ultrafiltration. As a control, the scattering of a nonconcentrated fraction of His-SpNOX was measured. The normalized scattering curves and that obtained from SEC-SANS are superimposed (Fig. S7), showing that the protein measured in static mode is monomeric. Downstream data analysis was performed with the scattering curve obtained with the best signal/noise ratio in static SANS and from the concentrated sample. To evaluate the effect of the His-tag, a sample of SpNOX was prepared in the same way but with thrombin cleavage of the His-tag before the last SEC elution in 21.4% D_2O. The scattering curves of the His-SpNOX and Tagfree-SpNOX are superimposed (Fig. 5 *A*). This confirms that the His-tag contribution is too small to be detected.

SANS analysis

SANS data analysis can be divided into three distinct parts. The first part consists of replotting the data under different classical graphs (Kratky plot, p(r), Guinier) to highlight specific particularities of the structure such as its flexibility, its maximum dimension, its global shape, and its Rg. This is a very robust analysis, but it is not sufficiently informative. Providing a few assumptions verified by our precharacterization (purity, monodispersity), we can reconstruct the shape of the molecule either "ab initio," using only SANS data, or by modifying a molecular model. Fig. 6 presents the SANS data and results obtained from their initial analysis (statistical information on SANS analysis are given in Table S3). Fig. 6, *B* and *C* show the Guinier analysis and the p(r) of the His-SpNOX and Tagfree-SpNOX curves. From the Guinier curves, we can extract an Rg of 30.2 ± 0.4 Å for the His-SpNOX sample and of 30.3 ± 0.3 Å for Tagfree-SpNOX. Both p(r) curves are also very similar and can be fitted with a very similar D_{max}, showing no effect of the polyHis tag on the global dimension of the protein in solution. The dimensionless Kratky plot of the diffusion data gives valuable information on the globularity and flexibility of the protein in solution (47). A compact, globular, monodomain protein will display a bell-shaped curve with a maximum at ($\sqrt{3}$, 1.1). The curves for SpNOX in solution, with or without tag, display a bell shape (Fig. 6 *D*), indicating that the protein is mainly compact but with a maximum slightly displaced from the ($\sqrt{3}$, 1.1) point, suggesting some flexibility and/or domain separation.

Comparison of SANS envelope to homology model

Good structural information for separated TM and DH domains of NOX proteins was made available by the x-ray crystallography of CsNOX (25). We used these structures as templates to generate a homology model of SpNOX TM and DH domain as described in the Materials and Methods (Fig. 7, *A* and *B*). The previously proposed docking of the separately crystallized CsNOX domains provides initial information regarding the relative position of the domains, but in the docked structure, the TM domain clashes with the predicted location of the adenosine phosphate part of FAD. The homology models of SpNOX that we built were also docked with reference to the docked CsNOX structure. The docked SpNOX domains also show clashes with FAD (Fig. 7 *C*) and, in addition, at the interface between the DH and TM domains. This implies that the hinge region between the two domains in the full-length CsNOX, and by extension SpNOX, is likely to be somewhat different from the predicted conformation in the docked model.

Fig. 7 *D* shows that our docked homology model (ribbon) is too compact to represent the solution structures obtained ab initio from SANS (surface or mesh). The TM domain is properly positioned in the ab initio envelope, but the space occupied by the ab initio model's cytosolic domain is much larger than the volume of the homology model's DH domain. Indeed, the homology model has a D_{max} of 85 Å and an Rg of 27.5 Å, significantly lower than the experimental values obtained above for the ab initio model (100 and 30.3 Å, respectively). Thus, it appears that SpNOX

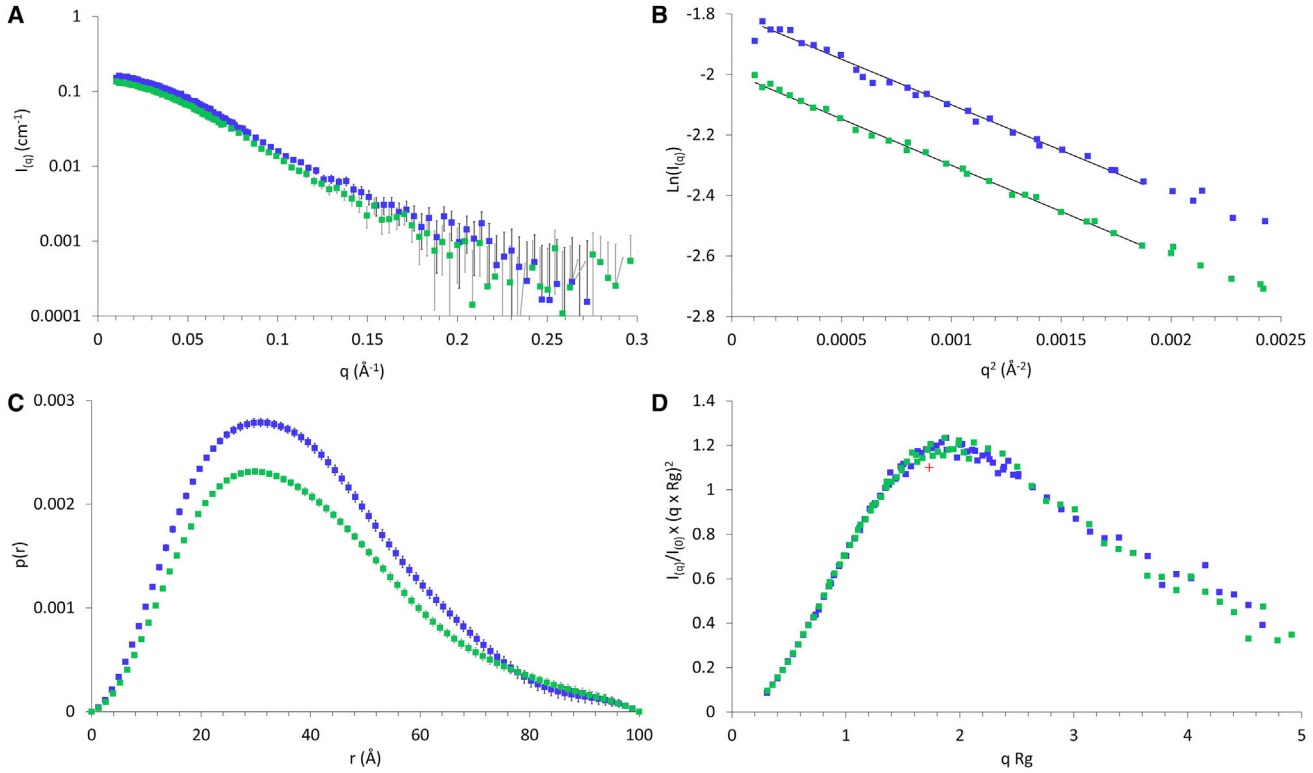

FIGURE 6 Analysis of the His-SpNOX (*blue*) and Tagfree-SpNOX (*green*) scattering data in 21.4% D_2O. (*A*) Logarithmic representation of the scattering curves in absolute scale. (*B*) Guinier analysis: Guinier representation of the low angle data and fits (*black line*) over an Rg × q range of 0.30–1.30. (*C*) Pair distance distribution function, p(r) calculated using the program GNOM and imposing a maximum r of 100 Å (*error bars* are represented). (*D*) Dimensionless Kratky plot of the data. The red cross corresponds to ($\sqrt{3}$; 1.1). To see this figure in color, go online.

undergoes a mass redistribution leading to a rearrangement between the TM and DH domain.

We used Pepsi-SANS software to refine the docked homology model to more closely conform to the experimentally produced full-length SANS model. The two domains of our docked SpNOX model were virtually separated to break potentially unrealistic contacts and to enable a greater range of motion of the domains relative to each other. This over-open model was submitted to Pepsi-SANS together with the SANS data. Keeping the TM domain fixed, the DH domain was allowed to move along the slowest normal modes, generating a large number of conformations (Fig. S8). The theoretical scattering curve of these conformations was calculated and compared with the experimental SANS data. Fig. 8 *A* shows the docked homology model, the over-open homology model, and the best fit homology model obtained from the flexible fitting process. The model-based approach results in a structure in which the DH and TM domains of SpNOX are not tightly apposed, but instead the protein is open in solution, which would provide accessibility to the interface between TM and DH domains (Fig. 8 *B*).

As expected, the TM domains of SpNOX from the docked model (*ribbon*) and from the ab initio envelope (*surface*) superimpose well (Fig. 8 *B*), whereas the DH domains of the two models occupy different positions. Notably, in the ab initio envelope, the DH domain fills a much larger volume. This conclusion agrees well with the ab initio reconstructed envelope being much larger than the homology model and some potential interdomain flexibility suggested by the Kratky plot (Fig. 6 *D*). Although this more open arrangement appears to be the conformation adopted by the protein in solution in our experimental conditions, the enzymatic functionality of SpNOX requires a close contact between the two domains to enable electron transfer from FAD to hemes. This implies that the open conformation is flexible enough to close, possibly upon substrate binding or another stimulus.

CONCLUSIONS

This work underlines the great potential for the use of the LMNG micelle as a general stealth carrier for future SANS studies of IMPs. It opens many future prospects for the study of membrane proteins and membrane protein complexes by SANS. The approach detailed here is complementary to the method developed by Maric et al. (7,8) and applied by Josts et al. (6) and Nitsche et al. (48) using nanodisks to stabilize membrane transporters. To cancel the nanodisk carrier contribution in their SANS experiments,

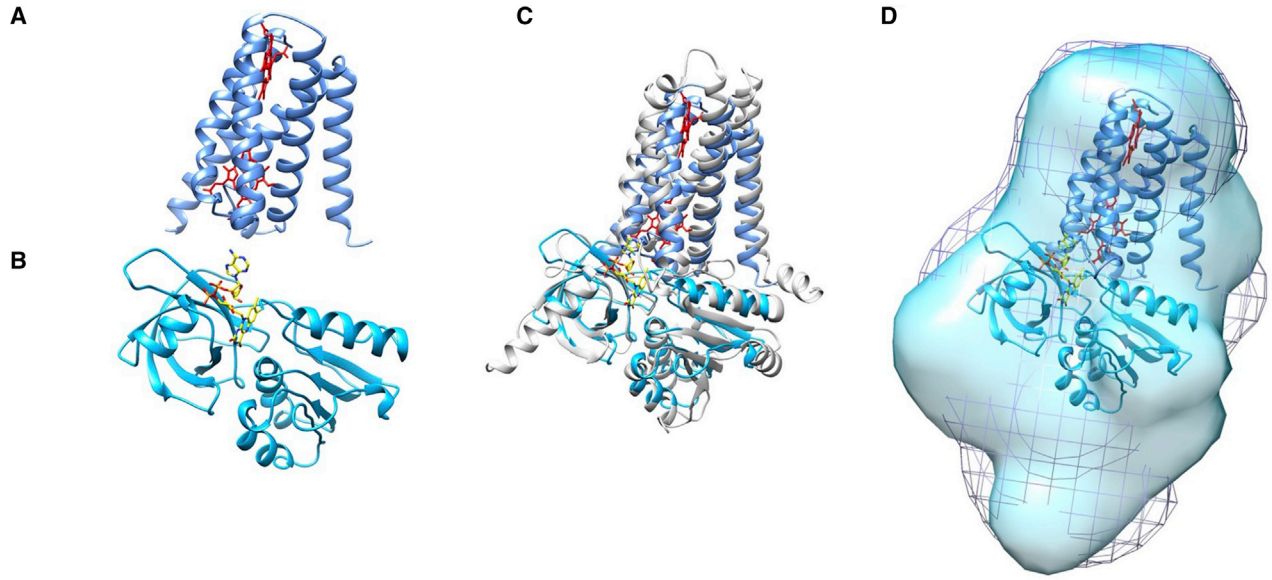

FIGURE 7 Homology model of (*A*) SpNOX TM domain, (*B*), DH domain, and (*C*) SpNOX docked model structure (*blue*) constructed using CsNOX docked model (*white*, based on docked PDB: 5O0T and PDB: 5O0X from Magnani et al. (25)) as a template. (*D*) Ab initio envelopes determined by SANS of His-SpNOX (*surface*) and Tagfree-SpNOX (*mesh*), calculated with the program Dammif. Both envelopes display a similar shape. They are superimposed with the full-length SpNOX model from (*C*). To see this figure in color, go online.

the authors used a stealth nanodisk, composed of matched-out deuterated lipids and a matched-out deuterated MSP invisible in 100% D_2O. The unlabeled membrane proteins to study were inserted into the deuterated nanodisks. The work described here used exactly the inverse labeling strategy in which the carrier, commercial LMNG detergent, is not labeled and the SpNOX protein to study is deuterated. In our case, we benefit from the unique properties of LMNG to be SANS invisible in 21.4% D_2O, and here, protein labeling increases the scattering contrast. These two complementary methods, stealth nanodisk or LMNG carriers, provide broad applicability to SANS experiments whatever the heterologous expression system used for the membrane protein recombinant production. Although production of deuterated protein is now straightforward using *E. coli,* it remains very challenging in higher eukaryotic expression systems. In such a case, the nanodisk approach will be preferred. Compared with using deuterated nanodisks for SANS, the method documented here is particularly attractive in cases in which the studied protein can be recombinantly produced in *E. coli*, as it uses a commercially available detergent that provides good stability to membrane proteins. Thanks to a well-established *E. coli* expression system for deuterated protein production, affording a high expression yield/cost ratio is now routinely reached.

Our work also highlights some new, to our knowledge, and unexpected properties of NOX enzymes. Comparison of homology modeling, ab initio envelopes, and normal mode analysis of the model shows significantly different structural and conformational properties of full-length SpNOX compared to the model structure obtained via docking of the isolated domains, at least when studied in absence of its electron donor, NAD(P)H. Of course, a general limit on the study of all membrane proteins resides in the use of a nonphysiological detergent environment. However, LMNG is so far the best environment for solubilized SpNOX in terms of protein activity and stability (11). The open structure obtained here, from the SANS analysis with the entire SpNOX in solution, suggests some flexibility to allow proper enzymatic function, which requires proximity of FAD to heme for electron transfer. Such interdomain flexibility would explain why the full-length NOX proteins are so difficult to crystallize, whereas the structure of the individual domains could be solved by x-ray crystallography. The unique structural information available to date was obtained from isolated domains of CsNOX, a prokaryotic algae homolog of human NOX5; no x-ray structure of a full-length NOX is yet available. The recent discovery of functional bacterial two-component systems composed of a membrane cytochrome b (e.g., MsrQ) and a cytosolic reductase (e.g., Fre) analogous to the respective domains in SpNOX (49) supports Sumimoto's suggestion (50) that NOX proteins evolved from the fusion of genes coding for the separate domains. Our observation that SpNOX is composed of two domains with structural autonomy and relative flexibility provides further support to this proposal.

The implications of a flexible linker between domains extend to structure-function studies of human NOXes. For example, only a handful of various chimeras linking the TM of one human isoform to the DH of a different isoform have been functional (51); electron transfer appears

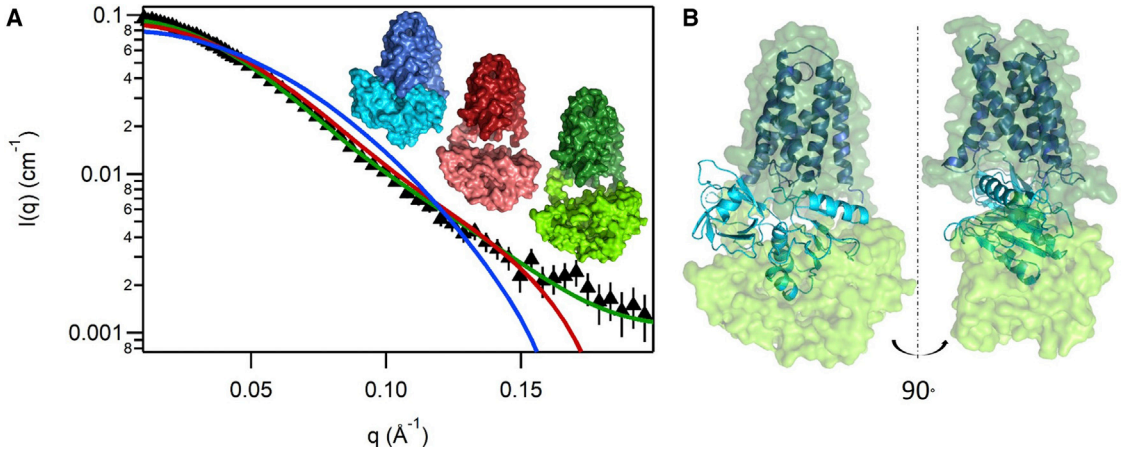

FIGURE 8 (*A*) Experimental SANS data of the Tagfree-SpNOX (*black triangles*) and calculated scattering curves (*lines*) of the SpNOX docked homology models (*blue*, I(0)/c = 0.13 cm^{-1} and Rg = 27.5 Å), the over-open SpNOX homology model used before fitting (*red*), and the best model resulting from flexible fitting along normal modes to the SANS data (*green*). Their respective χ^2-values are 39.4, 7.8, and 0.7. (*B*) The initial SpNOX docked model (*cartoon representation*) superimposed on best fit model (*green*, same as in *A*). The best fit model is depicted as a surface to prevent overinterpretation of the results from fitting to a ~10 Å low-resolution model. To see this figure in color, go online.

unusually sensitive to the exact structure of the interdomain linker. The B loop connecting TM helices 2 and 3 and the D-loop connecting TM helices 4 and 5 represent the most extensive locations in the TM domain available for interaction with the DH domain. The activity of chimeras in which the B and D loops are matched or mismatched to the DH isoform gave results apparently conflicting with experiments testing binding of B and D-loop synthetic peptides matched or mismatched to the DH domain (52); varying flexibility in the linkers of the chimeras may explain at least part of these discrepancies. If the flexibility of the interdomain linker and motion of the DH domain relative to the TM domain holds true for human NOXes, this provides a potential solution to the problem of the connection between component assembly and enzyme activity.

Our stability and activity measurements of SpNOX in the presence of detergent indicate that the observed relatively open conformation of the enzyme does not interfere with its activity. However, correct electron transfer requires an optimum alignment of the redox cofactors in the DH and TM domains (FAD and hemes, respectively). The openness of SpNOX is puzzling given that, in contrast to the eukaryotic NOX enzymes, SpNOX does not require activation by other factors. One possible explanation conjectures that NADPH binding within the DH domain induces proper docking of the DH onto the TM domain, thus promoting efficient electron transfer to the final electron acceptor. SANS experiments recently carried out on the PAN proteasome system (53) addresses conformation changes during catalysis. However, time-resolved SANS experiments cannot be envisaged to validate this hypothesis for SpNOX, because under the experimental conditions require, NADPH would be consumed too quickly. Further experiments using different approaches will be necessary to decipher the mechanism of electron flow in SpNOX and also to evaluate the extent to which SpNOX models eukaryotic NOX enzymes.

SANS data presented were recorded on Institut Laue-Langevin instrument D22 and are registered under DOIs 10.5291/ILL-Data.BAG-8-36, 10.5291/ILL-Data.BAG-8-37, and 10.5291/ILL-Data.INTER-382.

SUPPORTING MATERIAL

Supporting Material can be found online at https://doi.org/10.1016/j.bpj.2020.06.025.

AUTHOR CONTRIBUTIONS

F.F. conceived the study and coordinated the project and manuscript writing. A.V. and I.P.-H. prepared protein samples from recombinant expression to purification. A.V. performed the NanoDSF experiments and analyses. M.T. automated protein purifications. C.E. and A.M. defined SANS experiments. C.V. performed cloning and vector modifications for expression in deuteration medium. I.P.-H., A.L.R., and C.E. characterized sample quality via SEC-LS. M.M. and M.H. produced deuterated SpNOX sample. C.B., A.M., C.E., A.V., and F.F. collected SANS data. C.B., C.E., and A.M. conducted SANS data reduction and analysis. A.V. and S.M.E.S. made the homology model of SpNOX. S.G. adapted software for SANS data analysis and contributed to the normal mode analysis. A.V., C.B., A.L.R., C.E., A.M., and F.F. made the figures. C.B., C.E., A.M., and F.F. wrote the manuscript; S.M.E.S. contributed to its editing and evolution. Finally, all authors approved the final version of the manuscript.

ACKNOWLEDGMENTS

A.M. thanks Cy Jeffries for his critical reading, improvement suggestions, and support for the ab initio data analysis. All authors thank Bastien Exertier for his work to make Pepsi software available.

This work used the platforms of the Grenoble Instruct center (UMS 3518 CNRS-CEA-UJF-EMBL) with support from FRISBI (ANR-10- INSB-05-02) and GRAL (ANR-10-LABX-49-01) within the Grenoble Partnership for Structural Biology. This work was supported by the French Agence Nationale de la Recherche (ANR-16-CE92-0001) to C.E. and C.B. and (ANR-17-CE11-0013) to F.F., A.V., I.P.-H., and M.T. A.V. was supported through the Emergence program from the Université Grenoble Alpes; S.M.E.S. was supported by an invited professorship from Univ. Grenoble and through Emergence partner Kennesaw State University.

REFERENCES

1. Arinaminpathy, Y., E. Khurana, …, M. B. Gerstein. 2009. Computational analysis of membrane proteins: the largest class of drug targets. *Drug Discov. Today.* 14:1130–1135.
2. Breyton, C., F. Gabel, …, C. Ebel. 2013. Small angle neutron scattering for the study of solubilised membrane proteins. *Eur. Phys. J. E Soft Matter.* 36:71.
3. Denisov, I. G., and S. G. Sligar. 2017. Nanodiscs in membrane biochemistry and biophysics. *Chem. Rev.* 117:4669–4713.
4. Abla, M., G. Durand, …, B. Pucci. 2012. A diglucosylated fluorinated surfactant to handle integral membrane proteins in aqueous solution. *J. Fluor. Chem.* 134:63–71.
5. Breyton, C., A. Flayhan, …, C. Ebel. 2013. Assessing the conformational changes of pb5, the receptor-binding protein of phage T5, upon binding to its *Escherichia coli* receptor FhuA. *J. Biol. Chem.* 288:30763–30772.
6. Josts, I., J. Nitsche, …, H. Tidow. 2018. Conformational states of ABC transporter MsbA in a lipid environment investigated by small-angle scattering using stealth carrier nanodiscs. *Structure.* 26:1072–1079.e4.
7. Maric, S., N. Skar-Gislinge, …, L. Arleth. 2014. Stealth carriers for low-resolution structure determination of membrane proteins in solution. *Acta Crystallogr. D Biol. Crystallogr.* 70:317–328.
8. Maric, S., M. B. Thygesen, …, T. G. Pomorski. 2015. Biosynthetic preparation of selectively deuterated phosphatidylcholine in genetically modified *Escherichia coli*. *Appl. Microbiol. Biotechnol.* 99:241–254.
9. Chae, P. S., S. G. F. Rasmussen, …, S. H. Gellman. 2010. Maltose-neopentyl glycol (MNG) amphiphiles for solubilization, stabilization and crystallization of membrane proteins. *Nat. Methods.* 7:1003–1008.
10. Hardy, D., R. M. Bill, …, A. J. Rothnie. 2016. Overcoming bottlenecks in the membrane protein structural biology pipeline. *Biochem. Soc. Trans.* 44:838–844.
11. Breyton, C., W. Javed, …, C. Ebel. 2019. Assemblies of lauryl maltose neopentyl glycol (LMNG) and LMNG-solubilized membrane proteins. *Biochim. Biophys. Acta Biomembr.* 1861:939–957.
12. Debeurme, F., A. Picciocchi, …, M.-J. Stasia. 2010. Regulation of NADPH oxidase activity in phagocytes: relationship between FAD/NADPH binding and oxidase complex assembly. *J. Biol. Chem.* 285:33197–33208.
13. Li, X. J., F. Fieschi, …, M.-J. Stasia. 2007. Leu505 of Nox2 is crucial for optimal p67phox-dependent activation of the flavocytochrome b558 during phagocytic NADPH oxidase assembly. *J. Leukoc. Biol.* 81:238–249.
14. Beaumel, S., A. Picciocchi, …, M. J. Stasia. 2017. Down-regulation of NOX2 activity in phagocytes mediated by ATM-kinase dependent phosphorylation. *Free Radic. Biol. Med.* 113:1–15.
15. Grizot, S., J. Fauré, …, E. Pebay-Peyroula. 2001. Crystal structure of the Rac1-RhoGDI complex involved in nadph oxidase activation. *Biochemistry.* 40:10007–10013.
16. Grizot, S., F. Fieschi, …, E. Pebay-Peyroula. 2001. The active N-terminal region of p67phox. Structure at 1.8 A resolution and biochemical characterizations of the A128V mutant implicated in chronic granulomatous disease. *J. Biol. Chem.* 276:21627–21631.
17. Groemping, Y., K. Lapouge, …, K. Rittinger. 2003. Molecular basis of phosphorylation-induced activation of the NADPH oxidase. *Cell.* 113:343–355.
18. Marcoux, J., P. Man, …, F. Fieschi. 2010. p47phox molecular activation for assembly of the neutrophil NADPH oxidase complex. *J. Biol. Chem.* 285:28980–28990.
19. Honbou, K., R. Minakami, …, F. Inagaki. 2007. Full-length p40phox structure suggests a basis for regulation mechanism of its membrane binding. *EMBO J.* 26:1176–1186.
20. Lapouge, K., S. J. Smith, …, K. Rittinger. 2000. Structure of the TPR domain of p67phox in complex with Rac.GTP. *Mol. Cell.* 6:899–907.
21. Wilson, M. I., D. J. Gill, …, R. L. Williams. 2003. PB1 domain-mediated heterodimerization in NADPH oxidase and signaling complexes of atypical protein kinase C with Par6 and p62. *Mol. Cell.* 12:39–50.
22. Karathanassis, D., R. V. Stahelin, …, R. L. Williams. 2002. Binding of the PX domain of p47(phox) to phosphatidylinositol 3,4-bisphosphate and phosphatidic acid is masked by an intramolecular interaction. *EMBO J.* 21:5057–5068.
23. Ziegler, C. S., L. Bouchab, …, M. Erard. 2019. Quantitative live-cell imaging and 3D modeling reveal critical functional features in the cytosolic complex of phagocyte NADPH oxidase. *J. Biol. Chem.* 294:3824–3836.
24. Hajjar, C., M. V. Cherrier, …, J. Dupuy. 2017. The NOX family of proteins is also present in bacteria. *MBio.* 8:e01487-17.
25. Magnani, F., S. Nenci, …, A. Mattevi. 2017. Crystal structures and atomic model of NADPH oxidase. *Proc. Natl. Acad. Sci. USA.* 114:6764–6769.
26. Haertlein, M., M. Moulin, …, V. T. Forsyth. 2016. Biomolecular deuteration for neutron structural biology and dynamics. *Methods Enzymol.* 566:113–157.
27. Dunne, O., M. Weidenhaupt, …, V. T. Forsyth. 2017. Matchout deuterium labelling of proteins for small-angle neutron scattering studies using prokaryotic and eukaryotic expression systems and high cell-density cultures. *Eur. Biophys. J.* 46:425–432.
28. Artero, J. B., M. Härtlein, …, P. Timmins. 2005. A comparison of refined X-ray structures of hydrogenated and perdeuterated rat gammaE-crystallin in H_2O and D_2O. *Acta Crystallogr. D Biol. Crystallogr.* 61:1541–1549.
29. Katoh, K., J. Rozewicki, and K. D. Yamada. 2019. MAFFT online service: multiple sequence alignment, interactive sequence choice and visualization. *Brief. Bioinform.* 20:1160–1166.
30. Pei, J., B.-H. Kim, and N. V. Grishin. 2008. PROMALS3D: a tool for multiple protein sequence and structure alignments. *Nucleic Acids Res.* 36:2295–2300.
31. Waterhouse, A. M., J. B. Procter, …, G. J. Barton. 2009. Jalview version 2–a multiple sequence alignment editor and analysis workbench. *Bioinformatics.* 25:1189–1191.
32. Zhang, Y. 2008. I-TASSER server for protein 3D structure prediction. *BMC Bioinformatics.* 9:40.
33. Pettersen, E. F., T. D. Goddard, …, T. E. Ferrin. 2004. UCSF chimera–a visualization system for exploratory research and analysis. *J. Comput. Chem.* 25:1605–1612.
34. Hildebrand, P. W., A. Goede, …, R. Preissner. 2009. SuperLooper–a prediction server for the modeling of loops in globular and membrane proteins. *Nucleic Acids Res.* 37:W571–W574.
35. Xu, D., and Y. Zhang. 2012. Ab initio protein structure assembly using continuous structure fragments and optimized knowledge-based force field. *Proteins.* 80:1715–1735.
36. Xu, D., and Y. Zhang. 2013. Toward optimal fragment generations for *ab initio* protein structure assembly. *Proteins.* 81:229–239.
37. Johansen, N. T., M. C. Pedersen, …, L. Arleth. 2018. Introducing SEC-SANS for studies of complex self-organized biological systems. *Acta Crystallogr. D Struct. Biol.* 74:1178–1191.
38. Kline, S. R. 2006. Reduction and analysis of SANS and USANS data using IGOR Pro. *J. Appl. Cryst.* 39:895–900.

39. Konarev, P. V., V. V. Volkov, …, D. I. Svergun. 2003. PRIMUS: a Windows PC-based system for small-angle scattering data analysis. *J. Appl. Cryst.* 36:1277–1282.

40. Petoukhov, M. V., D. Franke, …, D. I. Svergun. 2012. New developments in the *ATSAS* program package for small-angle scattering data analysis. *J. Appl. Cryst.* 45:342–350.

41. Semenyuk, A. V., and D. I. Svergun. 1991. GNOM – a program package for small-angle scattering data processing. *J. Appl. Cryst.* 24:537–540.

42. Volkov, V. V., and D. I. Svergun. 2003. Uniqueness of ab initio shape determination in small-angle scattering. *J. Appl. Cryst.* 36:860–864.

43. Grudinin, S., E. Laine, and A. Hoffmann. 2020. Predicting protein functional motions: an old recipe with a new twist. *Biophys. J.* 118:2513–2525.

44. Trewhella, J., A. P. Duff, …, A. E. Whitten. 2017. 2017 publication guidelines for structural modelling of small-angle scattering data from biomolecules in solution: an update. *Acta Crystallogr. D Struct. Biol.* 73:710–728.

45. Seddon, A. M., P. Curnow, and P. J. Booth. 2004. Membrane proteins, lipids and detergents: not just a soap opera. *Biochim. Biophys. Acta.* 1666:105–117.

46. Martins de Oliveira, V., V. Godoi Contessoto, …, V. B. Pereira Leite. 2018. Effects of pH and salt concentration on stability of a protein G variant using coarse-grained models. *Biophys. J.* 114:65–75.

47. Durand, D., C. Vivès, …, F. Fieschi. 2010. NADPH oxidase activator p67(phox) behaves in solution as a multidomain protein with semi-flexible linkers. *J. Struct. Biol.* 169:45–53.

48. Nitsche, J., I. Josts, …, H. Tidow. 2018. Structural basis for activation of plasma-membrane Ca^{2+}-ATPase by calmodulin. *Commun. Biol.* 1:206.

49. Juillan-Binard, C., A. Picciocchi, …, F. Fieschi. 2017. A two-component NADPH oxidase (NOX)-like system in bacteria is involved in the electron transfer chain to the methionine sulfoxide reductase MsrP. *J. Biol. Chem.* 292:2485–2494.

50. Sumimoto, H. 2008. Structure, regulation and evolution of Nox-family NADPH oxidases that produce reactive oxygen species. *FEBS J.* 275:3249–3277.

51. Helmcke, I., S. Heumüller, …, R. P. Brandes. 2009. Identification of structural elements in Nox1 and Nox4 controlling localization and activity. *Antioxid. Redox Signal.* 11:1279–1287.

52. Jackson, H. M., T. Kawahara, …, J. D. Lambeth. 2010. Nox4 B-loop creates an interface between the transmembrane and dehydrogenase domains. *J. Biol. Chem.* 285:10281–10290.

53. Ibrahim, Z., A. Martel, …, F. Gabel. 2017. Time-resolved neutron scattering provides new insight into protein substrate processing by a AAA+ unfoldase. *Sci. Rep.* 7:40948.

Biophysical Journal, Volume *119*

Supplemental Information

Interdomain Flexibility within NADPH Oxidase Suggested by SANS Using LMNG Stealth Carrier

Annelise Vermot, Isabelle Petit-Härtlein, Cécile Breyton, Aline Le Roy, Michel Thépaut, Corinne Vivès, Martine Moulin, Michael Härtlein, Sergei Grudinin, Susan M.E. Smith, Christine Ebel, Anne Martel, and Franck Fieschi

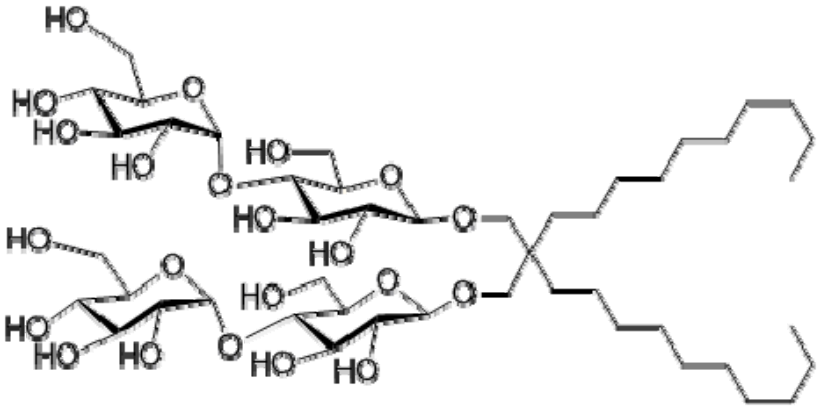

Scheme S1. Chemical structure of LMNG.

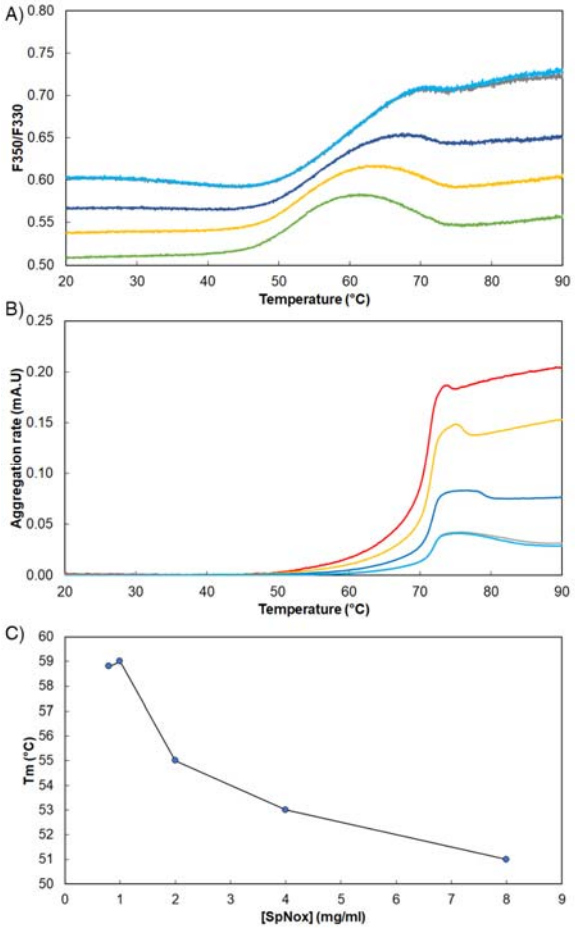

Figure S1: *A) Evolution of thermal unfolding curves with SpNOX concentrations (0.8, 1, 2, 4 and 8 mg mL^{-1}) at pH 7 in presence of 300 mM NaCl; B) Evolution of aggregation curves with SpNOX concentrations (0.8, 1, 2, 4 and 8 mg mL^{-1}) at pH 7 in presence of 300 mM NaCl. C) Tm dependency with SpNOX concentration from 0.8 to 8 mg mL^{-1} at pH 7 in presence of 300 mM NaCl.*

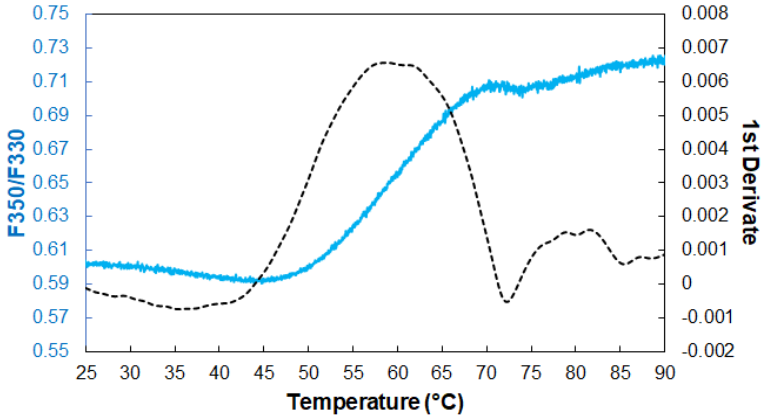

Figure S2: *Results of SpNOX thermal stability obtained with the optimal concentration of SpNOX (1 mg mL^{-1}) using NanoDSF. Thermal unfolding curve with SpNOX = 1 mg mL^{-1} (blue curve). 1st derivative of the thermal unfolding curve with SpNOX = 1 mg mL^{-1}*

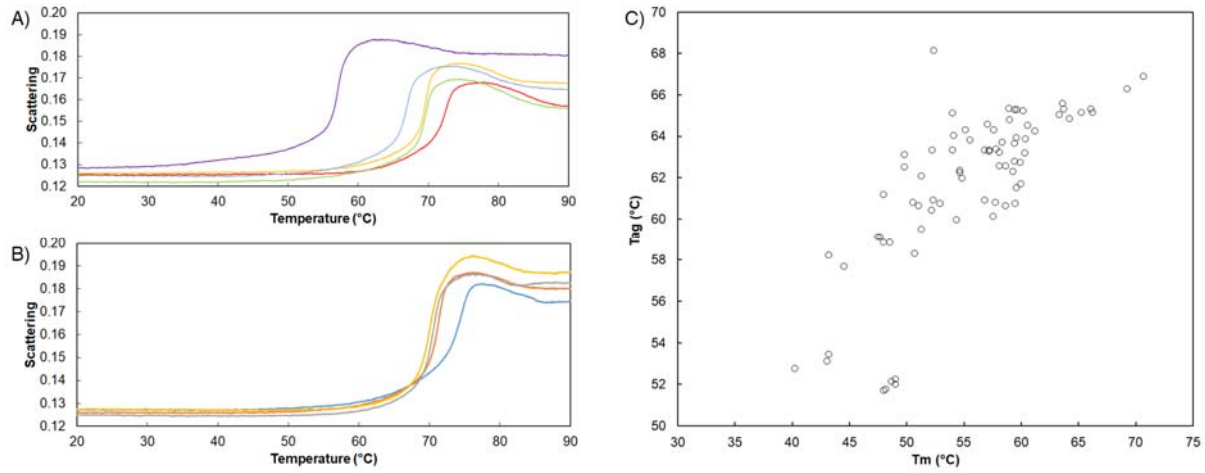

Figure S3: Scattering curves of SpNox as a function of pH and salt concentration. *(a) Scattering curves of SpNOX (0.8 mg mL^{-1}) in buffers containing 300 mM NaCl with various pHs: (dark blue) pH 9, (light blue) pH 8, (orange) pH 7, (green) pH 6, (red) pH 5. (b) Scattering curves of His-SpNOX (0.8 mg mL^{-1}) in elution buffer at pH 7 with NaCl concentrations of (dark blue) 25 mM, (light blue) 150 mM, (orange) 275 mM, (green) 520 mM. (c) Relationship between aggregation temperatures (Tag) extracted from scattering curves and the related melting temperatures (Tm) simultaneously determined in the same experimental conditions (same samples).*

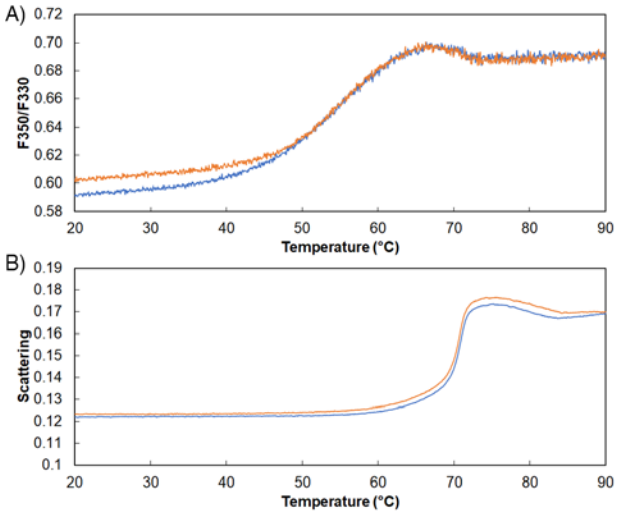

Figure S4: *Absence of effect of the presence (orange curve) of absence of FAD (10 µM) on SpNOX thermal stability and aggregation obtained with the optimal concentration of SpNOX (1 mg mL^{-1}) using NanoDSF.*

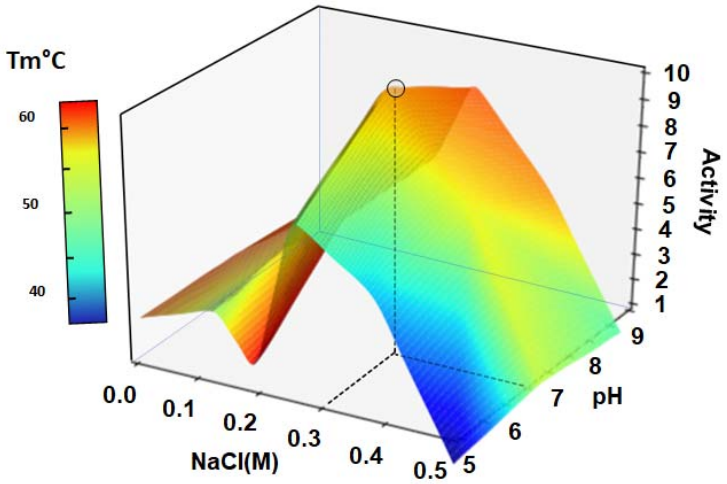

Figure S5: *3D representation of SpNOX specific activity and Tm (°C) as function of pH and NaCl concentration. The z-axis represents the SpNOX specific activity while the color represents the Tm (°C) value measured in same condition of pH and NaCl concentration. The dashed line represents the optimum condition (pH 7, 300 mM NaCl) to maximize both thermostability and activity.*

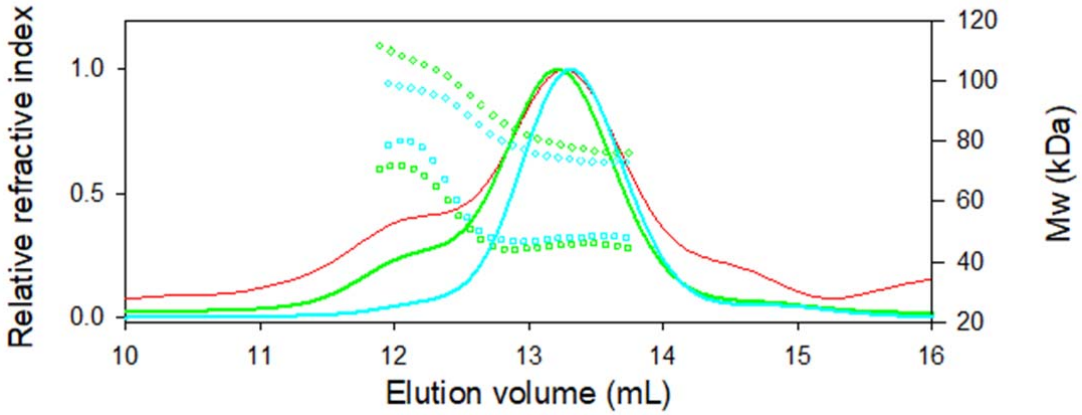

Figure S6: *SEC-LS analysis of the SpNOX fractions from SEC-SANS experiment. Elution profiles (continuous lines), and analysis in term of SpNOX (square) and LMNG (diamond) molar masses for fractions 12 (red), 13 (green) and 14 (cyan), see Figure 5.*

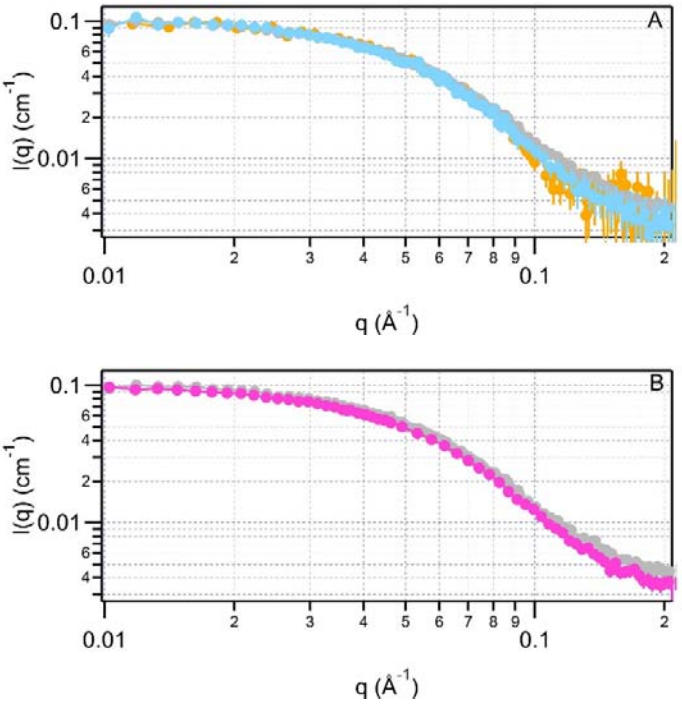

Figure S7*:* ***Scattering curves of SpNOX, in SEC-SANS and Static SANS, with and without His-Tag. A:*** *Superposition of the scattering curves of His-SpNOX, measured in SEC-SANS for boxes 3 to 5 (orange), and of an independent sample collected after size exclusion chromatography, before (blue) and after (grey) sevenfold concentration.* ***B:*** *Superposition of the scattering curves of His- SpNOX (grey), and Tagfree-SpNOX (pink), from size exclusion chromatography followed by concentration. All scattering curves were normalized to the forward scattering intensity calculated for 1 mg mL^{-1} monomer, and background adjustment to that of the SEC-SANS data. The solvent is 50 mM Tris-HCl pH 7, 300 mM NaCl, 10 µM FAD, 0.025 mM LMNG, 21.4 % D_2O.*

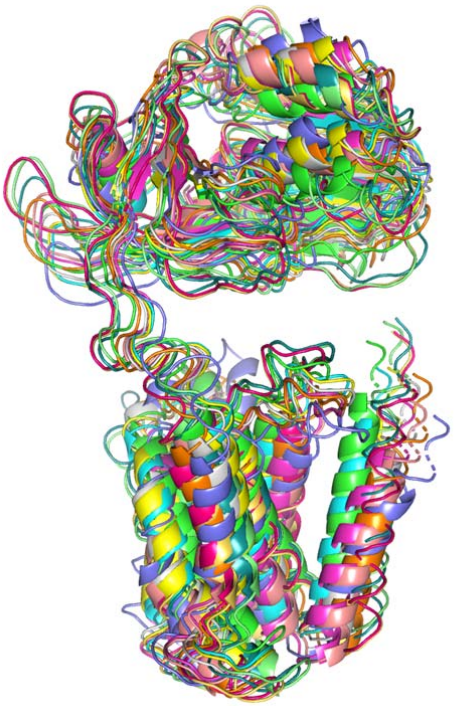

Figure S8: *Some of the conformations generated by Pepsi-SANS along Non-linear Normal Mode Analysis, starting from the artificially open model of Tag-free SpNOX. From these structures, the best fitting one is depicted in green in fig 8.*

Table S1 *: Neutron scattering length densities (SLD) and contrast match points (CMP) of LMNG, including hydrophobic/and hydrophilic sub-parts* [a]

	D_2O (%)			CMP ($\%D_2O$)	
	0	100	21.4	calculated	experimental
SLD Solvent (10^{-6} Å^{-2})	-0.56	6.4	0.93		
SLD LMNG (10^{-6} Å^{-2}) [b]	0.84	1.95	1.08	23.9	21.4
SLD Core (10^{-6} Å^{-2})	-0.30	-0.30	-0.30	3.7	
SLD anhydrous head (10^{-6} Å^{-2})	1.88	3.99	2.33	50.3	
fitted SLD hydrated head (10^{-6} Å^{-2}) [c,d]	1.134	5.048	1.97	55.5	
fitted shell hydration (%) [c,d]	30	44	33	8.0	

[a] *Most of the values are reported in Breyton, C., W. Javed, A. Vermot, C.-A. Arnaud, C. Hajjar, J. Dupuy, I. Petit-Hartlein, A. Le Roy, A. Martel, M. Thépaut, C. Orelle, J.-M. Jault, F. Fieschi, L. Porcar, and C. Ebel. 2019. Assemblies of lauryl maltose neopentyl glycol (LMNG) and LMNG-solubilized membrane proteins. Biochim. Biophys. Acta Biomembr. 1861: 939–957.*

[b] *calculated from the chemical formulae and the experimental partial specific volume of 0.797 ml* g^{-1}

[c] *from global fitting, in terms of core-shell cylinder, of SAXS and SANS data of 20 mM LMNG in* H_2O *and* D_2O

[d] *linked values*

Table S2: *Characterization of the fractions issued from SEC-SANS.*
SEC-LS, Activity assays, and Thin Layer Chromatography (TLC) experiments were done as in Breyton, C., et al (2019) Biochim. Biophys. Acta Biomembr. 1861: 939–957. MALDI TOF Mass Spectrometry experiment were done using a Autoflex maX (Bruker Daltonics), after diluting the samples five times in sinapinic acid.

	F12	F13	F14
Absorbance data			
SpNOX (mg mL^{-1})	0.05	0.55	1.17
A_{416}/A_{280}	1.2	1.5	1.9
SEC-LS data			
Monomer %	62	78	94
MW monomer (kDa)	65	48	50
Bound LMNG (g g^{-1})		1.7	1.5
MW shoulder (kDa)	84	74	82
Specific Activity			
(mol Cyt c reduced s^{-1} mol^{-1} SpNOX)		4.6	8
MALDI-TOF			
MW main peak (Da)	49980	49966	49896
MW minor peak (Da)	101633	101808	100372
TLC			
Total LMNG (mg mL^{-1})			2.8

Table S3*:* SANS sample, experiment, analysis, and results description for His-SpNOX and Tagfree-SpNOX.

(a) Sample details	His-SpNOX		Tagfree-SpNOX	
Organism	Streptococcus pneumoniae; expression in E. coli			
Source (Catalogue No. or reference)	Uniprot ID: Q8CZ28-1			
Description: sequence (including Uniprot ID + uncleaved tags), bound ligands/modifications, etc.	FAD-binding FR-type domain-containing protein ligand: flavoprotein (FAD), haemoprotein (iron) ; substrate not present in our experiment: NADPH			
Modifications:				
In blue: HisTag present only in His-SpNOX	HHHHHHHAGLVPRGSRSMEFSMKSVKGLLFIIASFILTLLTWMNTSPQFMIPGLALTSLSLTFILATRLPLLESWF HSLEKVYTVHKFTAFLSIILLIFHNFSMGGLWGSRLAAQFGNLAIYIFASIILVAYLGKYIQYEAWRWIHRLVYLAYIL GLFHIYMIMGNRLLTFNLLSFLVGSYALLGLLAGFYIIFLYQKISFPYLGKITHLKRLNHDTREIQIHLSRPFNYQSGQF AFLKIFQEGFESAPHPFSISGGHGQTLYFTVKTSGDHTKNIYDNLQAGSKVTLDRAYGHMIIEEGRENQVWIAGGI GITPFISYIREHPILDKQVHFYYSFRGDENAVYLDLLRNYAQKNPNFELHLIDSTKDGYLNFEQKEVPEHATVYMCG PISMMKALAKQIKKQNPKTELIYEGFKFK			
Deuteration level	70%			
Extinction coefficient ε 280 nm ($M^{-1}.cm^{-1}$)				
From quantitative aminoacid acid hydrolysis	107066			
SpNOX peptide chain (from ProtParam)	68760			
Optical Density at 280nm	3.36		2.98	
Concentration	1.51	2.35	1.29	2.02
Partial specific volume ($cm^3.g^{-1}$)	0.750			
Mean solute scattering length density ($.10^{10}$ cm^{-2})	5.178			
Mean solvent scattering length density ($.10^{10}$ cm^{-2})	0.929			
Mean scattering contrast ($.10^{10}$ cm^{-2})	4.249			
Molecular mass M from chemical composition of fully protonated form (Da)	48081		46527	
Volume from chemical composition	60062.9		58202.8	
Solvent composition and source	50 mM Tris-HCl pH 7, 300 mM NaCl, 5 mM LMNG, 10 µM FAD, 21.4% D_2O			

(b) SAS data collection parameters	His-SpNOX	Tagfree-SpNOX
Source, instrument and description or reference	Institut Laue Langevin, D22	
Proposal	BAG 8-36	
Wavelength (Å)	6 Å +/- 10%	
Beam geometry at sample (mm width x mm height)	7 x 10	
Source geometry (mm width x mm height)	40 x 55	
collimation length (m): sample detector distance (m)	2.8:2 and 5.6:5.6	
q-measurement range ($Å^{-1}$)	0.01-0.45	
Absolute scaling method	Direct: normalisation by flux at sample position	
Basis for normalization to constant counts	Normalisation to monitor count	
Exposure time (min)	30 min (5.6m) and 15 min (2m)	120 min (5.6m) and 45 min (2m)
Sample configuration including path length	1 mm thick Suprasil Quartz rectangular Hellma cuvettes (ref 100-1-40)	
Sample temperature (ºC)	7	
(c) Software employed for SAS data reduction, analysis and interpretation		
SAS data reduction to sample–solvent scattering, and extrapolation, merging, desmearing etc. as relevant	GRASP for data reduction; Igor with NCNR macros for solvent subtraction and merging	
Calculation of ε from sequence	Expasy/ProtParam	
Calculation of SLD and partial specific volume from chemical composition	BSLDC from Isis	
Basic analyses: Guinier, P(r), scattering particle volume	ATSAS: AutoRg and GNOM	
Atomic structure modelling (homology)	HD and TM domains independantly modeled using I-Tasser (closest	
Modelling of missing sequence from PDB files	D-loop (A110 and W121) reconstructed using SuperLooper. HisTag modeled using QUARK online	
Ab initio Modelling	ATSAS/DAMMIN	
Model-based shape reconstruction	Pepsi-SANS-NMA	
Molecular graphics	Pymol and chimera	
(d) Structural parameters	**His-SpNOX**	**Tagfree-SpNOX**
Guinier Analysis (reciprocal space)		
I(0) (cm^{-1})	0.17	0.14
err I(0) (cm^{-1})	0.0012	0.0008
Rg (Å)	30.21	30.26
err (Rg) (Å)	0.36	0.29
q-range ($Å^{-1}$)	0.012-0.042	0.012-0.042
Quality-of-fit parameter (with definition) χ^2 and fide	0.86	0.99
Expected I(0) (from BSLDC, 80% labile H exchanged)	0.12 0.18	0.10 0.15
Ratio I(0) measured / I(0) expected	1.44 0.93	1.42 0.91
P(r) analysis (real space)		
I(0) (cm^{-1})	0.17	0.14
apparent Rg (Å)	30.09	30.66
dmax (Å)	100	100
q-range ($Å^{-1}$)	0.01-0.25	0.01-0.25
Quality-of-fit parameter: χ^2/dof and Total quality es	0.84	0.88
Porod Volume ($Å^3$)	80073.9	88859.6
Ratio Porod volume/molecular volume	1.3	1.5

(e) Ab initio shape reconstruction	**His-SpNOX**	**Tagfree-SpNOX**
Method	DAMMIN online, slow mode, 20 replicates (all good fits and NSD<1); DAMAVER all, DAMFILT and DAMSTART with default parameters; DAMMIN in expert mode, from damstart output, with 25 harmonics and 80 knots	
q-range for fitting	0.01-0.25	
Symmetry/anisotropy assumptions	None	
Ambiguity measure a-score (Ambimeter)	2.053	1.591
χ^2 range for the 20 fits	0.497 to 0.503	0.549 to 0.553
P value, any other quality-of-fit parameters	1	1
Final χ^2 of refined model fit	0.5	0.5536
Final Model Filtered Volume ($Å^3$)	9.70E+04	1.06E+05
Final Model Rg (Å)	30.16	30.68
Final Model Dmax (Å)	104.1	104.9
(f) model-based shape reconstruction		
Method	Pepsi-SANS online, flexible fit	
q-range for fitting ($Å^{-1}$)	0.01-0.25	
Symmetry assumptions	None	
χ^2 range	2.057 to 0.552	10.66 to 0.668
Final χ^2 of best model fit	0.552	0.668
Final Model Rg (Å)	33.33	32.41
Final Model Fit $I_{(0)}$ (cm^{-1})	0.157	0.129
Domain/subunit coordinates and contacts, regions of presumed flexibility as appropriate	TM (Nter to Y191) was kept fix	
(g) Data and model deposition IDs		
SASDBD ID		SASDJ63